Bi-monthly • November - December • 2012

ISSN: 0976-2108

BARC NEWSLETTER

भाभा परमाणु अनुसंधान केंद्र
BHABHA ATOMIC RESEARCH CENTRE

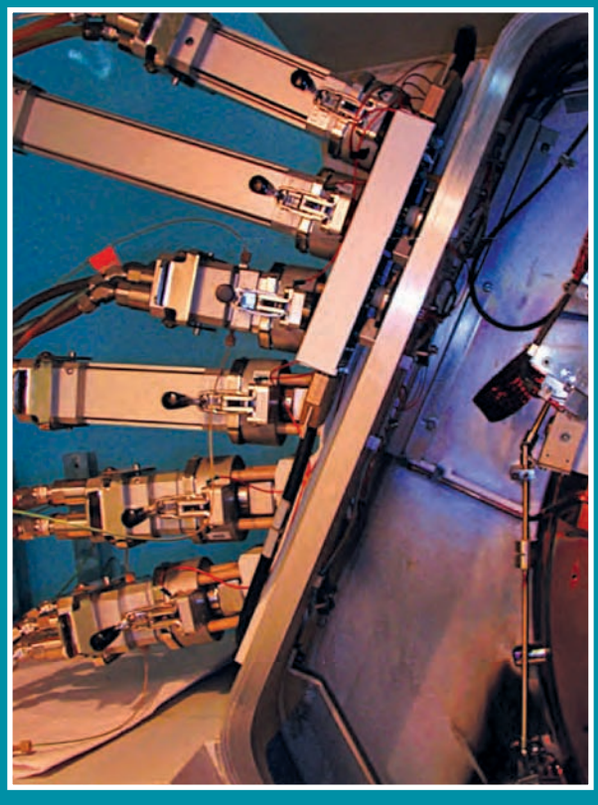

IN THIS ISSUE

CONTENTS

From the Editor's Desk

Welcome to the last issue of 2012. This year was quite eventful for the BARC Newsletter. For the first time, we introduced a new feature: "Brief Communications'. The response from our BARC fraternity was positive and encouraging. We also printed the BARC logo on the front cover of the July/August 2012 issue and later on all the subsequent issues.

As we take stock of the work of the Editorial Committee for the BARC Newsletter for the year 2012, we find that we have made good progress. We published a total number of 38 articles in many diverse areas of Nuclear Science and Technology and 26 Brief Communications. A list of all the published titles has been given at the end of this issue.

This issue carries seven articles. One on Materials drilling is an interesting peek into low-cost microwave drilling technique, used for various materials such as wood, glass, aluminium, copper, mild-steel (MS), animal bones specimens. The first Medical Cyclotron Facility (MCF) in the country is located at the Radiation Medicine Centre, Parel. This facility has recently completed ten years of successful operation. A glimpse into its operations has been covered in another article.

We hope to continue the good work and we solicit the continued cooperation and involvement of all BARC Scientists and Engineers. We also thank all our reviewers who have spared their valuable time in improving the quality of the published articles.

In the next year, we plan to create a web link on the SIRD Home Page for uploading articles, Brief Communications and also News and Events for all the regular issues of the BARC Newsletter. This will save a lot of time and effort.

Wishing you all a very productive and happy new year!

Dr. K. Bhanumurthy
On behalf of the Editorial Committee

Liquid Handling Robot

(Design, Manufacturing and Automation Group)

The Liquid Handling Robot is an indigenously developed, state of the art robotic system for performing liquid handling reactions on a large scale. The robotic system serves to automate the liquid handling job in different fields of research, like medical, biology, pharmacology, chemistry, etc. A liquid dispensing head carries out the job of collecting and dispensing the liquids in the desired volumes. The dispensing head along with a robotic positioning system driven by customized software interface helps in providing high throughput. They provide a modern approach to handle increasing numbers of samples with limited personnel resources and to minimize the possibility of errors during manual sample handling and preparation. They are also very helpful for handling potentially harmful solutions.

DRHR has developed the Liquid Handling Robot for extracting DNA from different types of cells by magnetic bead separation method. Magnetic beads are micron sized magnetic particles, to which only a particular type of molecules (in this case DNA molecules) gets attached. A specially designed magnet module is incorporated on the robot's platform to collect and re-suspend the magnetic beads within the solution, which is required at different stages of DNA extraction protocols such as lysing, elution etc. The magnetic bead separation method makes automated high yield DNA extraction possible without the need for any manual intervention.

Liquid handling robotic system consists of a motorized air-displaced 12 channel pipetting head, a magnet module, a precise two-axes robotic positioning system and a tray containing standard solution tubes array, fresh tip array & disposal station for used tips. The system is capable of handling liquids in the range of 30 to 300μl with repeatability less than 5%. A customized software interface has been developed for the user to define the reaction sequences using simple predefined steps like Aspiration, Dispensing, Tip Loading, Tip disposal, Mixing, Magnet, incubate, etc. The user also defines the solution tray configuration. The software keeps a check on liquid volume transactions and alerts the user for any volume disparity before executing it over the robot. It allows operator independent execution of the defined reaction. It also implements algorithms to minimize liquid splashing/sputtering while transportation, thus minimizing the chances of sample cross-contamination.

Fig. 1 shows the liquid handling robot system and Fig. 2 shows Graphical User Interface & Control Software.

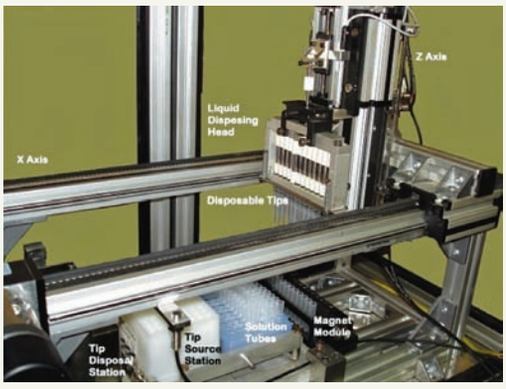

Fig. 1: Liquid Handling Robot System

Fig. 2: Graphical User Interface & Control Software

Integrated Environmental Radiation Monitor and Automatic Weather Station (ERM-AWS)

(Health Safety & Environment Group)

Online monitoring of atmospheric radiation and meteorological parameters are an integral input for handling any radiation emergency. HS&E group has been developing radiation detectors, with continuous improvements based on the advancement in technology and based on the requirements. BARC and ISRO under a collaborative program developed an integrated Environmental Radiation Monitor (ERM, developed under IERMON program) with Automatic Weather Station (AWS, developed by ISRO), as a single stand-alone system with solar powered battery backup and online data communication using ISRO satellite.

The indigenous cost effective system developed gives online hourly data on Wind Speed, Wind Direction, Air Temperature, Humidity, Rainfall, Earth's Net Radiation, Atmospheric Pressure and Environmental Gamma Radiation. In case of gamma radiation level exceeding a pre-set threshold level (accidental conditions), the system transmits data at a frequency of 5 minutes. The system has a central pole of 7 m height with sensors at various heights. The pole is supported by guy wires. A dedicated stand-alone satellite Earth Station has also been established at CTCRS, Anushaktinagar, Mumbai, to receive the data transmitted from ERM-AWS system.

The integrated online data transmitting ERM-AWS system is a useful tool for handling local site emergency and will provide valuable inputs for handling offsite nuclear emergency using decision support systems like IRODOS (Indian Realtime Online Decision Support System) at Nuclear Power Plants and at other locations.

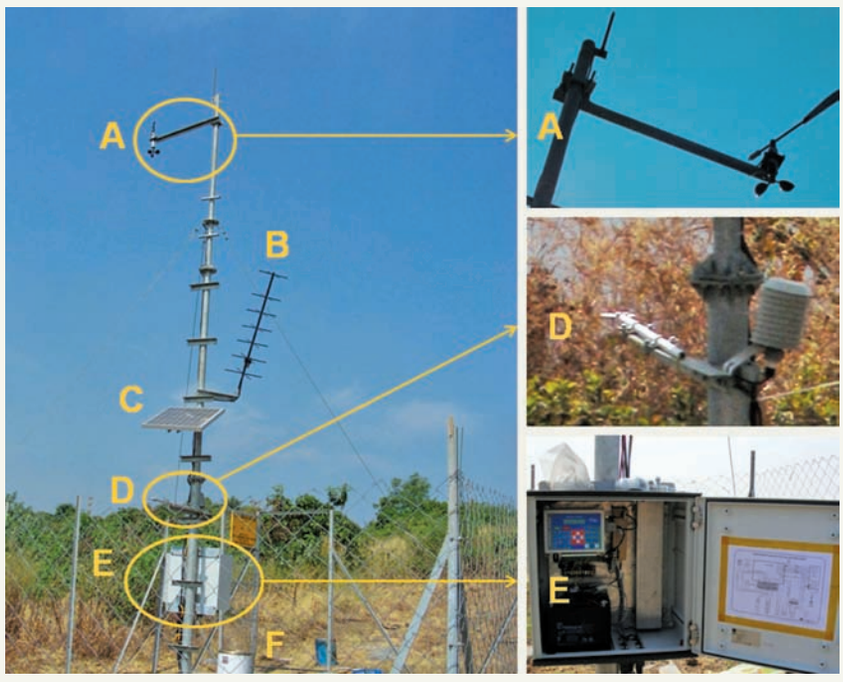

Fig. showing installed Integrated ERM-AWS system (A = Wind Vane and Cup Anemometer; B = Transmitting Antenna; C = Solar Panel; D = Temperature, Humidity and Earth's Net Radiation Sensors; E = Data Logger, Gamma Radiation Monitor and Battery; F = Rain Gauge)

Role of Cellular Redox Homeostasis in Modulation of Immune Responses

Rahul Checker, Deepak Sharma, Santosh K. Sandur and K. B. Sainis

Radiation Biology and Health Sciences Division, Bio-Medical Group

Abstract

Cellular redox status is described as the ratio of the inter-convertible oxidized and reduced form of specific redox couples of bio-molecules which exist in a dynamic equilibrium. Glutathione, cysteine and thioredoxin are three key regulators of cellular redox homeostasis. Any change in this equilibrium can alter cellular functions via modulation of signaling molecules like phosphatases or kinases and transcription factors. Further, immune responses are highly sensitive to changes in redox status inside as well as outside the cells. We have used phytochemicals to alter the redox homeostasis for desired modulation of immune responses. Our findings demonstrated that an antioxidant chlorophyllin augmented immune responses. On the contrary, a pro-oxidant plumbagin suppressed immune responses and exhibited potent anti-inflammatory activity in vitro and in vivo. The new targets identified in our studies may be useful for development of immuno-stimulatory or anti-inflammatory pharmaceuticals.

Cellular Redox Homeostasis

Molecular oxygen (O_2) is essential for the survival of all aerobic organisms. Reactive oxygen species (ROS), such as superoxide anion ($O_2^{\cdot-}$), hydrogen peroxide (H_2O_2), and hydroxyl radical (HO•), consist of radical and non-radical oxygen species formed by the partial reduction of oxygen. The radicals derived from oxygen represent the most abundant class of radical species generated in living system. There are exogenous and endogenous sources of cellular ROS. Exogenous sources include irradiation (UV, X- and γ-rays) and chemicals, such as redox-active metals (such as Fe and Cu) that enhance the Fenton/Haber–Weiss reaction (Trachootham et al. 2008). ROS are also generated through multiple sources inside the cells, such as the electron transport chain in mitochondria and through enzymes producing superoxide anion such as phagocytic and non-phagocytic NADPH oxidase, lipoxygenases and cycloxygenases. Two other oxidant species that are physiologically relevant are HOCl produced by the myeloperoxidase from neutrophils, and singlet oxygen ($^1O_2$) generated upon photosensitization and UVA irradiation (Roos et al. 2003). ROS can inflict damage to nucleic acids, proteins, and lipids and have been implicated in carcinogenesis, neurodegeneration, atherosclerosis, diabetes and aging (Ray et al. 2012). When ROS overwhelm the cellular antioxidant defense system, the cellular redox status is perturbed resulting in oxidative stress.

There are many redox couples in a cell that work together to maintain the redox environment; the GSSG/2GSH couple is the most abundant redox couple in a cell. The ratio of reduced to oxidized forms of glutathione reduced (GSH) / oxidized glutathione (GSSG), cysteine (reduced)/cystine (oxidized), thioredoxin reduced/ oxidized determines the cellular redox status. Under normal physiological conditions, cells maintain a reducing environment with a net redox potential ~ -220mV. A highly reduced environment with redox potential of about -240mV favors cellular growth and proliferation. However, under extreme oxidative stress conditions, this potential can increase upto -170mV leading to senescence or cell death. Further, cells have also developed a series of enzymatic and nonenzymatic

antioxidants. Enzymatic antioxidants comprise superoxide dismutase (SOD), which catalyze the dismutation of $O_2^{\cdot-}$ to H_2O_2, catalase that degrades H_2O_2 to H_2O and glutathione peroxidase (GPX) that converts peroxides to alcohols using reduced glutathione (GSH). Glutathione is the major thiol-disulfide redox buffer of the cell and its concentration in the cytosol ranges between 1–10 mM. It can directly scavenge $^{\cdot}OH$ and singlet oxygen by reaction with its thiol group. The thioredoxin system, composed of thioredoxin (TRX) and thioredoxin reductase, is another important antioxidant that act by reducing oxidized proteins (Trachootham et al. 2008).

Redox imbalance and immune system

The immune system maintains the integrity of the self and protects the host from infectious agents like bacteria, viruses, fungi, parasites and harmful insults. The immune system comprises of a diversity of serum proteins like complements, antibodies, and cytokines and effector cells like macrophages, polymorphonuclear cells and lymphocytes. Any change in the intracellular or extracellular redox state can perturb the normal course of immune response.

In a normal course of immune response, the phagocytes engulf pathogenic microbes and rapidly generate a variety of ROS species by a process called oxidative burst. These ROS species inactivate the engulfed bacteria or virus and also help in activation of lytic enzymes ensuring rapid killing of the pathogens. Antigen presenting cells like dendritic cells can influence the extracellular redox status by secreting out their GSH thus maintaining a reduced environment which is conducive for activation of antigen specific lymphocytes. An imbalance in intracellular generation of ROS species in phagocytes (neutrophils) increases the susceptibility of the host to a variety of otherwise non-pathogenic commensal bacteria and fungi leading to severe disorders like chronic granulomatous disease.

Excess ROS can alter protein structure and function by modifying critical amino acid residues, inducing protein dimerization, and interacting with Fe-S moieties or other metal complexes. The sulfhydryl group (-SH) of a single cysteine residue may be oxidized to form sulfenic (-SOH), sulnic ($-SO_2H$), sulfonic ($-SO_3H$), or S-glutathionylated (-SSG) derivatives. Such alterations may decrease the activity of an enzyme if the critical cysteine is located within its catalytic domain or inhibit the DNA binding ability of a transcription factor if it is located within its DNA-binding motif. Further, depending on the level of ROS, different redox-sensitive transcription factors are activated and coordinate distinct biological responses. A low oxidative stress induces Nrf2, a transcription factor implicated in the transactivation of gene coding for antioxidant enzymes. An intermediate amount of ROS triggers an inammatory response through the activation of NF-κB and AP-1, and a high level of oxidative stress induces disruption of mitochondrial membrane potential resulting in cell death.

These signaling pathways induced during modulation of cellular redox status have been intensely studied in immune responses primarily because lymphocytes are often subjected to changes in ROS levels during inammatory response, which can, in turn, inuence a number of signaling pathways. For example, at a site of inammation, H_2O_2 is produced by activated macrophages and neutrophils at an estimated rate of $2–6 \times 10^{-4}$ μM/h per cell and T cells may be exposed to 10–100 μM H_2O_2 in a physiological environment (Lander 1997). Secondly, it is now clear that the activation of T cells through their antigen receptors increases the level of intracellular ROS that, instead of being toxic, can actually play a positive role in controlling signaling pathways that lead to T cell proliferation.

The last two decades have seen a surge in the field of research associated with the immunomodulatory activities of dietary antioxidants and their role in preventing many human diseases. Several contrasting reports about the immnuo-stimulatory as well as immunosuppressive activities of phytochemicals have appeared recently. Based on

these observations, we have extensively studied the modulation of immune responses in response to redox alterations by phytochemicals. Plant derived molecules which act as either anti-oxidants or pro-oxidants in cellular systems were employed to study their ability to modulate immune responses both in vitro and in vivo and their mechanism of action has been elucidated.

A) Anti-oxidants as immunomodulators

An antioxidant is a molecule capable of slowing down or preventing the oxidation of other molecules. Even though several studies have reported the effects of redox modulation on immune responses the relationship between oxidative stress and the pathobiology of these diseases is not clear, largely due to a lack of understanding of the mechanisms by which ROS function in both normal physiological and diseased states. Chlorophyllin (CHL) is a water-soluble mixture of sodium-copper salts of green plant pigment chlorophyll, the ubiquitous photosynthetic green pigment present in food materials of plant origin as well as in nutritional supplements such as extracts from *Spirulina* and *Chlorella vulgaris*. Chlorophyll has been credited with several beneficial properties and CHL has proved to be better than the parent compound as evident from studies employing different model systems. It has chemopreventive, antimuatgenic and anticarcinogenic properties. The anti-oxidant and immunomodulatory properties of chlorophyllin elucidated in our laboratory are summarized in Table 1.

B) Modulation of immune responses by pro-oxidants

Cellular redox status plays an important role in the biological effector functions of lymphocytes and leukocytes. Exposure of T cells to oxidizing agents like H_2O_2, xanthine/xanthine oxidase has been shown to suppress T cell activation, proliferation, and cytokine production via suppression of NF-κB (Pahlavani and Harris 1998). Thus, we hypothesized that altering the redox balance of cells leads to modication of critical signaling molecules required for activation of lymphocytes. Plumbagin (5-hydroxy-2-methyl-1,4-naphthoquinone) is found in the plants of Plumbaginaceae, Droseraceae, Ancestrocladaceae, and Dioncophyllaceae families. The root of *Plumbago zeylanica* (also called Chitrak), a major source of plumbagin, has been used in traditional Indian medicine since 750 BC as an antiatherogenic, cardiotonic, hepatoprotective, and neuroprotective agent. Plumbagin has been shown to exert several therapeutic biological effects including anticancer, antiproliferative, chemopreventive, chemotherapeutic, and radiosensitizing properties in experimental animals as well as in tumor cells in vitro (Padhye et al. 2010). Lately, plumbagin was shown to inhibit constitutive as well as inducible NF-kB activation and NF-kB regulated genes in tumor cells. It also inhibited DNA binding ability of NF-8κB (Sandur et al. 2006). Based on these observations, we speculated that plumbagin may show immunomodulatory effects and might have significant clinical application in prevention of inflammatory disorders. The immunomodulatory properties of plumbagin were elucidated and are summarized below in Table 2. Its mechanism of action and in vivo efficacy was also evaluated and included in Table 2.

CONCLUSION: It is well established that any perturbation in the immune regulatory mechanisms may result in several undesired outcomes including self-tissue destruction, autoimmunity, allergy, chronic inflammation and cancer. One major thrust area of current clinical research is to devise novel strategies for immunosuppression which may be achieved by depleting lymphocytes, diverting lymphocyte traffic or blocking lymphocyte response pathways. Immunosuppressive drugs have three effects: the therapeutic effect (suppressing rejection), undesired consequences of immunodeficiency (infection or cancer) and toxicity to other tissues. The immunosuppressive regimens currently employed involves the use of multiple drugs such as inhibitos of transcription (Cyclosporin A,

tacrolimus), inhibitors of nucleotide synthesis (azathioprine, mycophenolate mofetil, mizoribine, leflunomide) and inhibitors of growth factor signal transduction (sirolimus, leflunomide).

Thus, development of novel strategies of immune intervention would be key to therapeutic management of inflammation. Our studies provide evidence use of redox modifiers (anti-oxidants and pro-oxidants) for modulation of immune responses in vivo. These studies underscore the crucial role of ROS and redox balance in lymphocyte activation and the mechanism(s) involved therein. Further, we also recognize the importance of plant derived phytochemicals as modulators of cellular redox balance which can have significant application towards management of immune responses for therapeutic benefits.

References

1. Boloor, K. K., J. P. Kamat, and T. P. Devasagayam. 2000. Chlorophyllin as a protector of mitochondrial membranes against gamma-radiation and photosensitization. *Toxicology* 155: 63-71.
2. Checker, R., D. Sharma, S. K. Sandur, S. Khanam, and T. B. Poduval. 2009. Anti-inflammatory effects of plumbagin are mediated by inhibition of NF-kappaB activation in lymphocytes. *Int Immunopharmacol* 9: 949-58.
3. Checker, R., D. Sharma, S. K. Sandur, G. Subrahmanyam, S. Krishnan, T. B. Poduval, and K. B. Sainis. 2010. Plumbagin inhibits proliferative and inflammatory responses of T cells independent of ROS generation but by modulating intracellular thiols. *J Cell Biochem* 110: 1082-93.
4. Jia, Y., J. Jing, Y. Bai, Z. Li, L. Liu, J. Luo, M. Liu, and H. Chen. 2011. Amelioration of experimental autoimmune encephalomyelitis by plumbagin through down-regulation of JAK-STAT and NF-kappaB signaling pathways. *PLoS One* 6: e27006.
5. Kohli, V., D. Sharma, S. K. Sandur, S. Suryavanshi, and K. B. Sainis. 2010. Immune responses to novel allergens and modulation of inflammation by vitamin K3 analogue: a ROS dependent mechanism. *Int Immunopharmacol* 11: 233-43.
6. Kumar, S. S., R. C. Chaubey, T. P. Devasagayam, K. I. Priyadarsini, and P. S. Chauhan. 1999. Inhibition of radiation-induced DNA damage in plasmid pBR322 by chlorophyllin and possible mechanism(s) of action. *Mutat Res* 425: 71-9.
7. Kumar, S. S., B. Shankar, and K. B. Sainis. 2004. Effect of chlorophyllin against oxidative stress in splenic lymphocytes in vitro and in vivo. *Biochim Biophys Acta* 1672: 100-11.
8. Lander, H. M. 1997. An essential role for free radicals and derived species in signal transduction. *Faseb J* 11: 118-24.
9. Padhye, S., P. Dandawate, M. Yusufi, A. Ahmad, and F. H. Sarkar. 2010. Perspectives on medicinal properties of plumbagin and its analogs. *Med Res Rev*.
10. Pahlavani, M. A., and M. D. Harris. 1998. Effect of in vitro generation of oxygen free radicals on T cell function in young and old rats. *Free Radic Biol Med* 25: 903-13.
11. Poosarla, A., N. R. D, R. R. Athota, and V. G. Sunkara. 2011. Modulation of T cell proliferation and cytokine response by Plumbagin, extracted from Plumbago zeylanica in collagen induced arthritis. *BMC Complement Altern Med* 11: 114.
12. Ray, P. D., B. W. Huang, and Y. Tsuji. 2012. Reactive oxygen species (ROS) homeostasis and redox regulation in cellular signaling. *Cell Signal* 24: 981-90.
13. Roos, D., R. van Bruggen, and C. Meischl. 2003. Oxidative killing of microbes by neutrophils. *Microbes Infect* 5: 1307-15.
14. Sandur, S. K., H. Ichikawa, G. Sethi, K. S. Ahn, and B. B. Aggarwal. 2006. Plumbagin (5-hydroxy-2-methyl-1,4-naphthoquinone) suppresses NF-kappaB activation and NF-kappaB-regulated gene products through

modulation of p65 and IkappaBalpha kinase activation, leading to potentiation of apoptosis induced by cytokine and chemotherapeutic agents. *J Biol Chem* 281: 17023-33.

15. Sharma, D., S. S. Kumar, R. Raghu, S. Khanam, and K. B. Sainis. 2007a. Differential modulation of mitogen driven proliferation and homeostasis driven proliferation of T cells by rapamycin, Ly294002 and chlorophyllin. *Mol Immunol* 44: 2831-40. Sharma, D., S. S. Kumar, and K. B. Sainis. 2007b. Antiapoptotic and immunomodulatory effects of chlorophyllin. *Mol Immunol* 44: 347-59.
16. Trachootham, D., W. Lu, M. A. Ogasawara, R. D. Nilsa, and P. Huang. 2008. Redox regulation of cell survival. *Antioxid Redox Signal* 10: 1343-74.

Table 1: Antioxidant and immunomodulatory properties of chlorophyllin

	Activity	Method	Result	Reference
ANTIOXIDANT ACTIVITY				
1	Radical Scavenging (hydroxyl)	Pulse Radiolysis	direct reaction of •OH with CHL $6.1\pm0.4\times10^{9}$ M^{-1} s^{-1} Rate constant	(Kumar et al. 1999)
2	Scavenging of radiation derived radicals from deoxyribose (ROO•)	Pulse Radiolysis	direct reaction of ROO• with CHL $5.0\pm1.3\times10^{7}$ M^{-1} s^{-1} Rate constant	(Kumar et al. 1999)
3	Radioprotective activity in cell free system	Plasmid protection assay	Dose dependent inhibited radiation-induced single strand breaks	(Kumar et al. 1999)
4	Inhibition of radiation induced lipid peroxidation	4-hydroxynoneal, TBARS, protein oxidation	Inhibition of 4-hydroxynoneal, TBARS and protein oxidation by CHL	(Boloor et al. 2000, Kumar et al. 2004)
5	Scavenging of radiation derived intracellular ROS in vitro and in vivo	oxidation of (H2DCF-DA)	CHL inhibited the increase in intracellular ROS in lymphocytes	(Kumar et al. 2004)
6	Radiation induced apoptosis	Propidium Iodide staining	CHL protected against radiation-induced apoptosis in lymphocytes.	(Kumar et al. 2004)
7	Radiation induced immunosuppression	Mitogen induced proliferation	CHL inhibited radiation-induced suppression of T cell proliferation	(Kumar et al. 2004)
8	Antioxidant enzyme activities (SOD, catalase and GPX)	Enzyme activity measurement	CHL increased catalase and GPX activities but not SOD	(Kumar et al. 2004)
IMMUNOMODULATORY ACTIVITY				
9	Lymphocyte proliferation	Mitogen induced proliferation	CHL inhibited lymphocyte proliferation in vitro	(Sharma et al. 2007b)
10	Activation induced cell death	Propidium Iodide staining	CHL protected against mitogen activation induced cell death	(Sharma et al. 2007b)
11	Expression of anti-apoptotic proteins (bcl-2 & bcl-xl)	RT-PCR analysis	CHL enhanced the expression of apoptosis-related genes bcl-2 and bcl-xL in lymphocytes	(Sharma et al. 2007b)
12	Effect on spleen size and the number of PEC	Flow cytometry	Increase in the spleen size following CHL administration Increase in the number of CD3+ T, CD 19+ B cells, CD 4+ T cells, CD 8+ T cells, CD 14+ macrophages	(Sharma et al. 2007b)
13	Phagocytic activity of peritoneal macrophages	Flow cytometry	Macrophages from CHL treated group showed higher phagocytic activity (60%).	(Sharma et al. 2007b)
14	Humoral Immune responses	plaque forming cell (PFC) assay	Frequency of PFC increased almost two-fold in CHL treated immunized	(Sharma et al. 2007b)
15	Adaptive immune responses	Delayed type hypersensitivity	DTH response was further enhanced in SRBC immunized mice treated with CHL	(Sharma et al. 2007b)
16	Cytokine secretion	ELISA	CHL treated cells did not show any decrease in IL-2 production or IFN-γ production as compared to Con A stimulated cells	(Sharma et al. 2007a)
17	T cell activation	Flow cytometry	CHL inhibited expression of CD25 and CD69 in activated cells	(Sharma et al. 2007a)
18	Homeostasis driven proliferation (HDP) of CD4+ T cells	Flow cytometry	Inhibitory action of CHL on HDP of CD4+ T cells	(Sharma et al. 2007a)

Studies on Self-diffusion of Radiotracer Tagged Counterions and Water in Ion-exchange Membranes

A.K. Pandey and A. Goswami
Radiochemistry Division

Summary

Self-diffusion coefficients (SDC) of counterions and water in different ion-exchange membranes have been measured to study the effects of matrix parameters on diffusion process. Radiotracers are ideal tool for studying SDCs in the Ion-exchange membrane. We have developed a "non-stationary radiotracer method" to measure SDC. The measured SDC provides valuable information about the physical parameters that govern the transport process In this article, a glimpse of the work that is being carried out in Radiochemistry Division is given.

Introduction

Membranes are defined as discrete, thin interface that separates two phases and moderate the permeation of various ions/chemical species in a selective manner. Ion-exchange membranes have fixed-charge sites and equivalent mobile counterions to maintain electro-neutrality. The mobile counterions are exchangeable. The ion-exchange membranes are semipermeable as they allow counterions to pass through while co-ions are restricted by Donnan exclusion process.[1-3] The self-diffusion coefficient (SDC) is a true measure of mobility of ions in the ion-exchange membranes, and governs the transport properties of the membrane. Techniques such as radiotracer permeation, ion-exchange, conductivity/impedance measurements and pulsed field gradient nuclear magnetic resonance spectroscopy [PFG-NMR] have been used to determine self-diffusion coefficients of ions and water in the ion-exchange membranes.[4,5] Radiotracer and PFG-NMR methods directly yield the well-defined self-diffusion coefficients.

In our lab, work has been carried out overseveral years to determine SDCs of counterions and water in different ion-exchange membranes using radiotracers. The major objective of the studies has been to understand the parameters that govern SDC of diffusing spices in the membrane.

Isotopic-exchange Method

To understand diffusional transport of ions in Nafion, Yeager et al. measured SDC of Na^+ and Cs^+ counterions in Nafion-117 membrane using radiotracer permeation method.[6] The disadvantage of radiotracer permeation method is that it requires several permeation experiments to deduce single value of self-diffusion coefficient and requires the use of carrier-free radiotracer. To overcome this limitation, we have developed the non-stationary radiotracer method.[5]

The non-stationary radiotracer method is essentially based on the analysis of kinetics of isotopic-exchange between membrane and equilibrating solution using an analytical solution of Fick's second law. For a plane sheet of membrane with appropriate initial and boundary conditions, the solution is given as:[5,7]

$$n(t_k) = n^* [1-(8/\pi^2)\{\exp(-D^m \pi^2 t_k / L^2) + (1/9) \exp(-9 D^m \pi^2 t_k / L^2) + ...\}] \quad (1)$$

where n* is the total amount of the radiotracer ions in the membrane at equilibrium (t=∞). In the case of desorption experiment, that is, radiotracer diffusing out of the membrane, n* represents the total radiotracer ions in the salt solution at equilibrium (t=∞). D^m and L are self-diffusion coefficient (SDC) of counterion and thickness of membrane, respectively.

Experimental Method

The measurements of radiotracer-exchange rates of $(M^{n+})_{mem} \rightleftharpoons (*M^{n+})_{aq}$ (sorption) or $(M^{n+})_{mem} \rightleftharpoons (*M^{n+})_{aq}$(desorption) (*tagged with radiotracer) have been carried out using 2x2 cm^2 pieces of the membrane samples. The equilibrating salt solution containing membrane sample is stirred vigorously (≈500 rpm) to avoid the aqueous film diffusion. The amount of radiotracer counterions sorbed/desorbed from the membrane sample has been monitored by taking out aqueous/membrane sample from the equilibrating solution at regular time intervals, and counting its radioactivity. The γ-activity in membrane/aqueous sample has been counted in a well-type NaI(Tl) γ-ray detector coupled to multichannel analyzer. The α/β-activity in aqueous sample has been counted with a liquid scintillation counter employing a Dioxane-based cocktail scintillator. The radiotracers like ^{24}Na, ^{42}K, ^{65}Zn etc. have been obtained by irradiating known amounts of their stoichiometric compounds for appropriate times in the APSARA reactor at BARC, Mumbai, India. The other radiotracers like ^{45}Ca, ^{137}Cs, ^{133}Ba, $^{85,89}Sr$, ^{110m}Ag etc. have been procured from the Board of Radiation and Isotope Technology, Mumbai, India.

The variation of $n(t_k)$ as a function of equilibration time t_k has been analyzed by a non-linear least-squared fit of eq. 1 with both n* and D^m_i as free parameters. Thus, single experiment yields a value of SDC. The representative fitted profiles of experimental isotopic-exchange rates are shown in Fig.1.

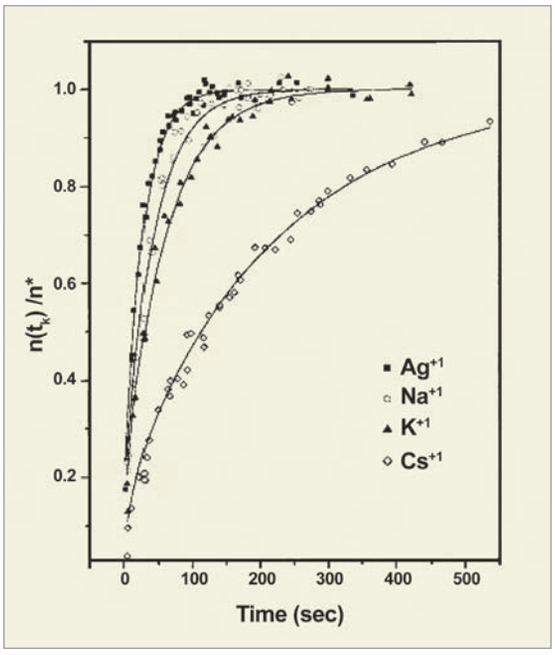

Fig.1: Variation of fractions of the radiotracer monovalent ions in the Nafion-117 membrane as a function of time *t*. (Ref.5).

The variation of SCD in Nafion-117 for different radiotracer tagged counterions as a function of time for attaining of 99% equilibrium is shown in Fig. 2. This gives an estimate of time required for completion of experiment for a given value of SDC. Except for

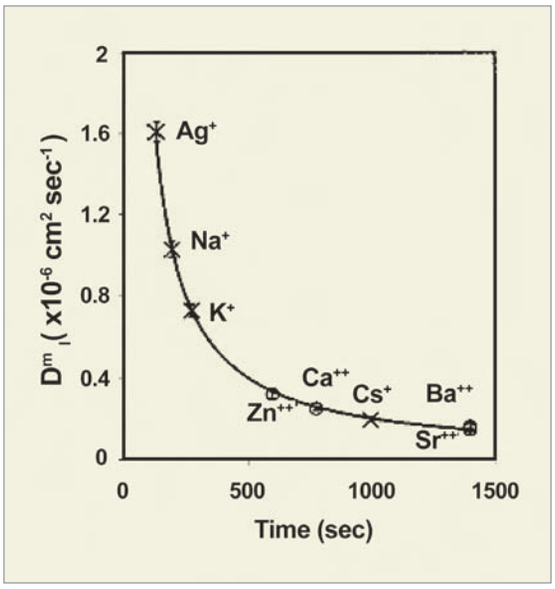

Fig.2: Self-diffusion coefficients of different ions vs. time required for 99% attainment of equilibrium in the Nafion-117 membrane (Ref.5).

Cs^+, M^+ counterions requires less equilibration time compared to M^{2+} counterions, showing higher electrostatic interactions with fixed charge sites for the bivalent ions.

Results

Correlation of Selectivity with Self-diffusion Coefficients

The selectivity coefficients (K^M_H) of the ions in the membrane are plotted against the measured SDCs (D^m_i) in Fig. 3. It is evident from Fig. 3 that K^M_H decreases systematically with increase in D^m_i for both monovalent and divalent ions. The selectivity of the ions having the same charge follows the sequence of decreasing radii of the hydrated ions. In general, it appears that a membrane having higher selectivity for a counterion would have lower SDC for the same counterion leading to slower transport rate.

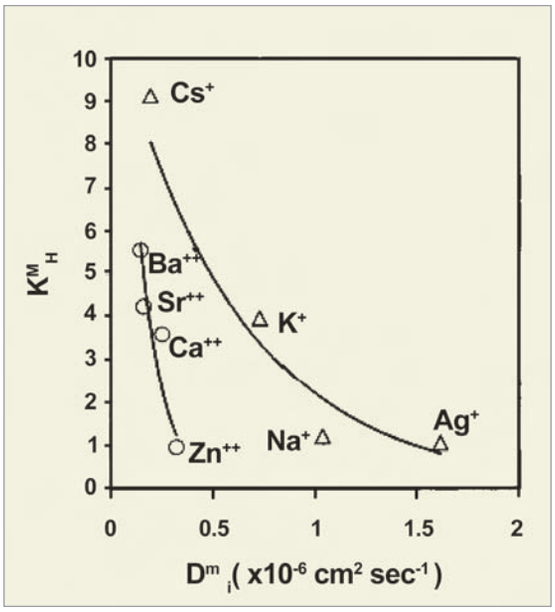

Fig. 3: Plot of selectivity coefficient (K^M_H) vs. SDC in the Nafion-117 membrane (Ref.5).

Effects of Free-volume on Self-diffusion

Diffusion of ions is obstructed by polymer chains and occurs through the region containing water in a membrane. Thus, the ions have to take tortuous path through the membrane, and the tortuosity factor is a function of polymer volume fraction. According to free volume theory of Yasuda et al.[8]

$$\frac{D_i^m}{D_i^o} = \frac{g(\varphi)}{Z_i} \exp[-b\frac{V_P}{1-V_P}] \qquad (2)$$

where D^m_i and D^o_i are SDC of counterions in membrane and water, respectively, Z_i is the charge on counterion, b is a slope parameter and $V_p/(1-V_p)$ is the polymer volume fraction. '$g(\phi)$' is a preexpoential factor introduced to take into account the electrostatic interaction of an ion with the fixed charge sites of the ion-exchange membrane. The value of $g(\phi)/Z_i$ is unity in eq. 2 for neutral species like water. The ratio of SDC of water molecules in membrane ($D^m_{H_2O}$) to SDC of water molecules in water ($D^o_{H_2O}$) thus provides a measure of tortuosity factor in the membrane. Therefore, $D^m_{H_2O}$ in different ionic forms of Nafion-117 have been measured using tritiated water (HTO) to study the tortuosity factor for different ionic forms of the membrane.[9] For measuring $D^m_{H_2O}$, the desorption of tritiated water from membrane sample in required ionic form has been monitored by taking out samples from equilibrating water for liquid scintillation counting, and analyzing ($(HTO)_{mem} \rightleftharpoons (H_2O)_{aq}$) exchange in terms of eq. 1.[9] The polymer volume fraction (V_p) of the membrane samples in different ionic forms was calculated from the volume of the water in the membrane and the volume of the wet membrane sample as described elsewhere.[9]

The plots of ln (D^m_i / D^o_i) and ln ($D^m_{H_2O}$) with polymer volume fraction $V_p/(1-V_p)$ are shown in Fig. 4a and Fig. 4b, respectively. D^m_i and $D^m_{H_2O}$ were experimentally measured using isotopic-exchange method as described above, and values of D^o_i and $D^o_{H_2O}$ were taken from literature as given in our publication.[5,9] $D^m_{H_2O}$ is not normalized with $D^o_{H_2O}$ as it is a fixed quantity ($2.5x10^{-5}$ cm^2/s). It is seen from Fig. 4 that ln (D^m_i / D^o_i) and ln ($D^m_{H_2O}$) vary linearly as a function of $V_p/(1-V_p)$, which is in accordance with free volume theory (eq. 2).The variation of ln ($D^m_{H_2O}$) with $V_p/(1-V_p)$ signifies systematic change in tortuosity with polymer volume fraction. However, the variation ln (D^m_i / D^o_i) with $V_p/(1-V_p)$ indicates

variation of both electrostatic interactions and tortuosity factor with polymer volume fraction. Separate lines clearly suggest that morphologies of Nafion samples in monovalent and multivalent counterionic forms are different. Variation of $D^m_{H_2O}$ in different cationic forms of the membrane is much less (3.87×10^{-6} cm^2/s in H^+-form to 1.50×10^{-6} cm^2/s in Cs^+-form) compared to D^m_i, indicating water channels in Nafion-117 are very well connected even with lowest water content in Cs^+-form.

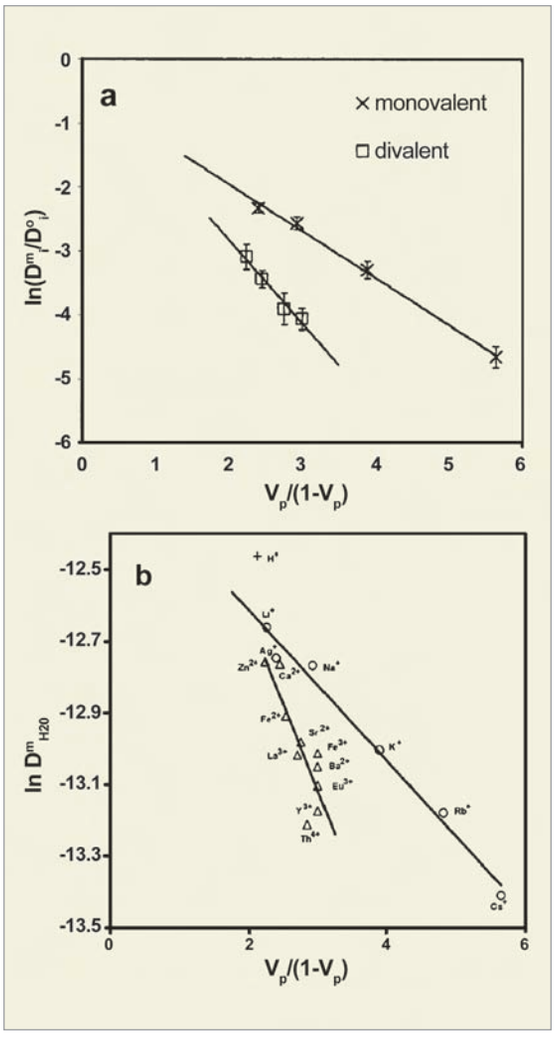

Fig.4: (a) Plots of ln (D^m_i / D^o_i) of the counterions (Ag^+,Na^+, K^+, Cs^+, Zn^{2+}, Ca^{2+}, Sr^{2+}, Ba^{2+}) (Ref. 5), and (b) ln ($D^m_{H_2O}$) (Ref. 9) in different ionic form of the membrane against the polymer volume fraction function [$V_p/(1- V_p)$].

Effects of Electrostatic Interaction between Counterions and Fixed-charge Sites

It is possible from eq. 2 to evaluate electrostatic interaction parameter $g(\phi)$ using parameter "b" obtained from slope in variation of ln ($D^m_{H_2O} / D^o_{H_2O}$) with $V_p/(1-V_p)$.[9] This is based on the fact the morphology is same in both the cases. The variation of $g(\phi)$ for different counterions as a function $V_p/(1-V_p)$ is shown in Fig. 5.

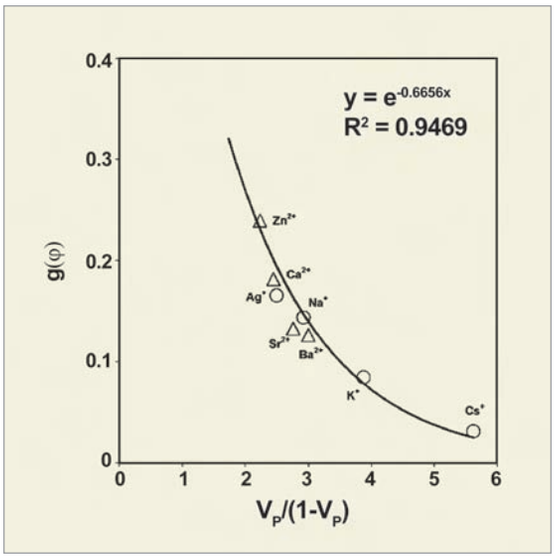

Fig.5: Variation of electrostatic interaction parameter $g(\phi)$ obtained from eq. 2 for self-diffusion of ions in membrane as a function of $V_p/(1-V_p)$ (Ref.9).

It is evident from this plot that $g(\phi)$ is also a exponential function of $V_p/(1-V_p)$. It is expected that the $g(\phi)$ would depend on spacing of fixed charge in the diffusion channels in membrane and effective interaction distance between fixed charge sites and mobile counterions. The effective interaction distance between mobile counterions and the fixed charge site are dependent on the hydration radius of counterions in the membrane. Since V_p in Nafion-117 membrane depends on the hydration characteristics of counterions, both these factors correlate $V_p/(1-V_p)$ to $g(\phi)$. It is important to note that lower value of $g(\phi)$ indicates higher strength of electrostatic interaction. Thus, Cs^+ ions having lower

SDC has lower value of $g(\phi)$ indicating its strong electrostatic interactions with fixed ion-exchange sites in the membrane.

Counterions-exchange Studies in Nafion-117

Counterions-exchange method can be used to determine SDC when appropriate radiotracer of counterions is not available or acidic condition is required to prevent hydrolysis of counterions in equilibrating solution. For brief description of this method, consider the process of ion-exchange between an ion "A" initially present in the plane sheet of the membrane and an ion "B" initially present in the solution as:

$$A^{Z_A}(\mathrm{m}) + B^{Z_B}(\mathrm{aq}) \rightleftharpoons A^{Z_A}(\mathrm{aq}) + B^{Z_B}(\mathrm{m})$$

where Z_A and Z_B are the charges on the ions A and B, 'm' and 'aq' represent the membrane phase and solution phase, respectively. Based on Nernst-Planck (N-P) theory, the diffusion equation describing the time and space dependence of the ion concentration c_i in the membrane can be written as:[10-12]

$$\frac{\partial c_i}{\partial t} = \frac{\partial}{\partial x}\left[D_{AB} \frac{\partial c_i}{\partial x} \right] \qquad (3)$$

where the inter-diffusion coefficient D_{AB} is given by:

$$D_{AB} = \frac{D_A D_B (Z_A^2 C_A + Z_B^2 C_B)}{(D_A Z_A^2 C_A + D_B Z_B^2 C_B)} \qquad (4)$$

where D_A and D_B are self-diffusion coefficients of interchanging counterions A and B whose concentrations in membrane phase are represented by C_A and C_B , respectively. During the course of ion-exchange, C_A, C_B and D_{AB} change with time and thus eq. 3 becomes non-linear. A numerical solution of eq. 3 has been obtained by finite difference method, and used for calculation of fractional attainment of exchange equilibrium (F(t)) vs. $t^{1/2}$ for fixed Z_A, Z_B and (D_A/D_B). The quantity F(t) is also experimentally measured and fitted with solution of eq. 3 to obtain the ratio D_A/D_B. If SDC of one inter-exchanging counterion is known, the value of SDC of other counterion can be deduced from this ratio. The details are given in Ref. 11 & 12. The experimental method is same as that used for non-stationary radiotracer method except that exchanging counterions between equilibrating solution and membrane are different.

Forward and Reverse Counterions-exchange

A consequence of Nernst-Planck is that forward and reverse counterions-exchange profiles are not same. It can be seen from Fig. 6 that the counterion exchange rate is altered by the mobility of the ion entering into the membrane. Thus, the rate of exchange of an ion present in the membrane, which is having higher diffusivity, is retarded by a slow diffusing ion entering the membrane. Similarly, the rate of exchange of a slow diffusing ion present in the membrane is accelerated by a faster diffusing ion entering the membrane. For example, Na^+ self-diffusion coefficient is higher (1.03×10^{-6} cm^2/s) than that for Eu^{3+} ions (0.045×10^{-6} cm^2/s) in Nafion-117. Therefore, the kinetics of counterions-exchanges follow the trend $Na^+_{(mem)} \rightleftharpoons Na^+_{(aq)}$, > $Na^+_{(mem)} \rightleftharpoons Eu^{3+}_{(aq)} > Eu^{3+}_{(mem)} \rightleftharpoons Na^+_{(aq)} > Eu^{3+}_{(mem)} \ll Eu^{3+}_{(aq)}$.[12] The counterions-exchange rate predicted by Nernst-Planck theory does not always match with experiment as seen from the studies of counterions-exchanges involving H^+ ions.[11] The N-P theory has been found to be reasonably accurate for predicting the the kinetics of the reverse ion exchange $M^{n+}_{(mem)} \rightleftharpoons H^+_{(aq)}$, but fails for the forward ion exchange $H^+_{(mem)} \rightleftharpoons M^{n+}_{(aq)}$. Contrary to the prediction of the N-P theory, the kinetics of forward exchanges of Cs^+, Cu^{2+}, and Eu^{3+} with H^+ ions in the Nafion-117 membrane have been found to be independent of the metal ions.[11] This shows that the self-diffusion coefficients of the counterions in Nafion-117 can be obtained only from the analysis of reverse exchange kinetics based on the N-P equation.

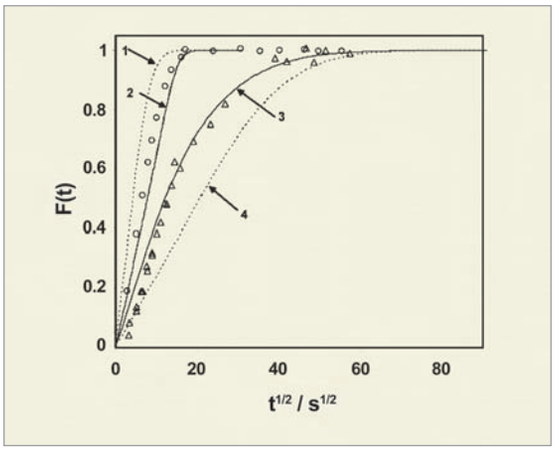

Fig. 6: Fractional attainments of counterions-exchanges equilibriums in Nafion-117. The symbols represent the experimental data on $Na^{+}_{(mem)} \rightleftharpoons Eu^{3+}_{(aq)}$ (O) and $Eu^{3+}_{(mem)} \rightleftharpoons Na^{+}_{(aq)}$ (D) exchanges. Lines 1, 2, 3 and 4 represent the calculated profiles of $Na^{+}_{(mem)} \rightleftharpoons Na^{+}_{(aq)}$, $Na^{+}_{(mem)} \rightleftharpoons Eu^{3+}_{(aq)}$, $Eu^{3+}_{(mem)} \rightleftharpoons Na^{+}_{(aq)}$, and $Eu^{3+}_{(mem)} \rightleftharpoons Eu^{3+}_{(aq)}$ exchanges, respectively (Ref.12).

The SDC value of Li^{+} ion (for which no suitable radiotracer exists) in Nafion-117 membrane has been obtained by analyzing its exchange kinetics with radiotracer tagged Na^{+} or Cs^{+} counterions.[12] Unlike other counterions, drastic difference in diffusion mobility of Li^{+} ions during forward and reverse exchanges has been obtained, wich is attributed to the weak electrostatic interactions of Li^{+} ions with the fixed exchange sites in Nafion membrane.

Effects of Self-diffusion Coefficients on Competitive Diffusion of Counterions

Multi-component diffusion studies have been carried out to understand how the kinetic selectivity and thermodynamic selectivity affect the membrane transport process.[13] Studies have been carried out in Nafion-117, using two cations, namely Na^{+} and Cs^{+}, having widely different self-diffusivity and selectivity.[14] At all compositions of $Na^{+}+Cs^{+}$ ions in the equilibrating solutions, the Na^{+} ion concentration has been found to pass through a maximum in the membrane, while the Cs^{+} ion concentration continuously increased till equilibrium is reached. This has been explained as being due to higher diffusivity but lower selectivity of Na^{+} ions than Cs^{+} ions. An attempt has been made to reproduce the time profile of the competitive diffusion for both the ions using the modified form of Maxwell–Stefan formalism. Fig. 7 shows the time evaluation of the spatial distributions of Na^{+} and Cs^{+} ions in Nafion-117 membrane as obtained from the numerical solution of Maxwell–Stefan equation.

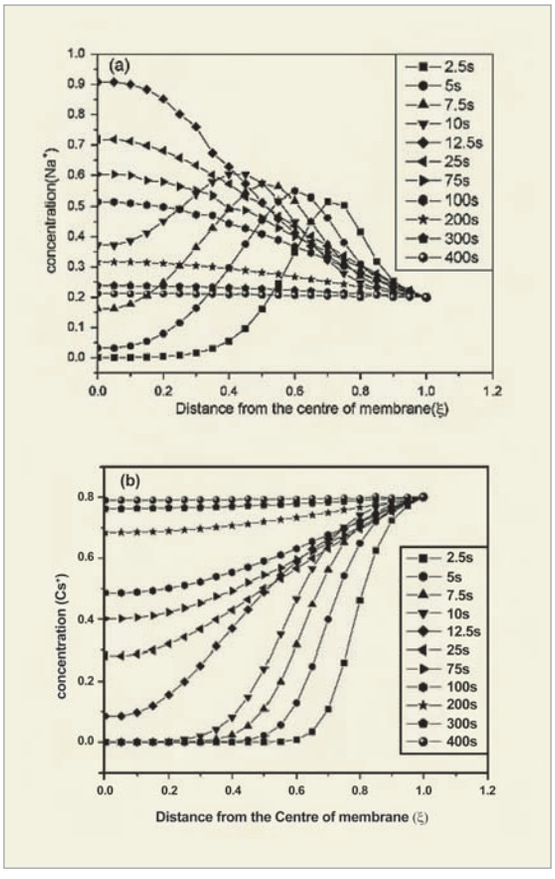

Fig. 7: The spatial distribution of competing ions in the membrane as a function of transient uptake time during diffusion from a solution containing Na^{+}/Cs^{+} in 1:1 ratio. (a) Na^{+} and (b) Cs^{+} (Ref.14) calculated using Maxwell–Stefan equations.

Effect of Ionic-composition of Membrane on Self-diffusion Coefficients

In order to understand the effect of ionic composition on SDC, the SDC of Na^{+}, Cs^{+}, and Ba^{2+} in Nafion-117 has been determined using two radiotracers and by varying ionic compositions of $Na^{+}+Cs^{+}$, $Na^{+}+Ba^{2+}$, $Cs^{+}+Ba^{2+}$ and $Ag^{+}+Ba^{2+}$ ions in the membrane.[15] The values of SDC have been obtained by analyses of isotopic-exchange profiles using eq.1. It has been observed that the

SDCs do not change in mixed binary counterionic forms except those involving $Na^{+} \rightleftharpoons Ba^{2+}$ and $Ag^{+} \rightleftharpoons Ba^{2+}$ exchanges. This has been attributed to different transport pathways of cations in Nafion-117 membrane.

Effect of Speciation in Aqueous Samples on Self-diffusion Coefficients

Self-diffusion coefficient also provides a new approach for speciation studies as it is highly sensitive to chemical form of the diffusing species. Isotopic and ion-exchange kinetics of mercury ions in Nafion-117 membrane in the presence of Cl^{-} and NO_3^{-} in solution have been studied to see the effect of anions on SDC of metal ions.[16] The speciation diagrams, calculated as a function of pH, show wide divergence of species present in $HgCl_2$ and $Hg(NO_3)_2$ solution. SDCs corresponding to different chemical form of mercury cations entering in the Nafion-117 membrane from equilibrating $HgCl_2$ and $Hg(NO_3)_2$

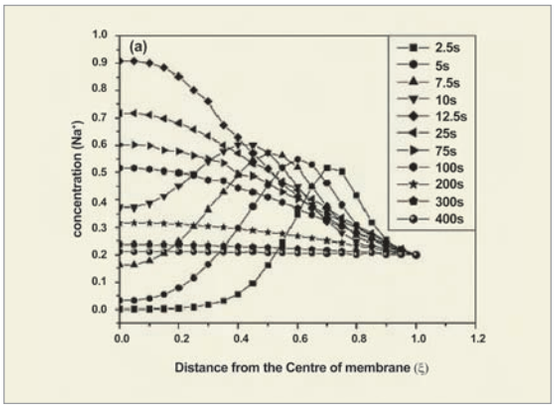

Fig.8: Variation of fractions of the radiotracer of monovalent ($HgCl^{+}$) and divalent (Hg^{2+}) mercury ions in the Nafion-117 membrane (Ref.16).

solutions have been obtained. The isotopic-exchange profiles are given in Fig.8.

The results indicate that mercury ions diffuse into the membrane as monovalent cation ($HgCl^{+}$) from $HgCl_2$ solution while as divalent ion (Hg^{2+}) from $Hg(NO_3)_2$ solution. This gives rise to an interesting possibility of developing a method for speciation studies based on diffusion mobility of the ions in the ion-exchange membrane.

Self-diffusion in Polymer Inclusion Membrane

Tailor-made polymer inclusion membranes (PIMs) for different applications have been developed in our lab. In order to understand role of matrix forming polymer, plasticizer and concentration of carrier (extractant) in transport process, SDCs of ions and water have been studied in PIMs prepared by physical immobilization of the trioctylmethylammonium chloride (Aliquat-336) in the plasticized matrix of cellulose triacetate (CTA). The plasticizers having different dielectric constant and viscosity are used to vary the local environment of the membrane matrix. AFM image of a PIM shown in Fig. 9 indicates that it is homogeneous non-porous membrane. Thus, transport of ions through this class of membrane is mediated by the carriers immobilized in plasticized matrix.

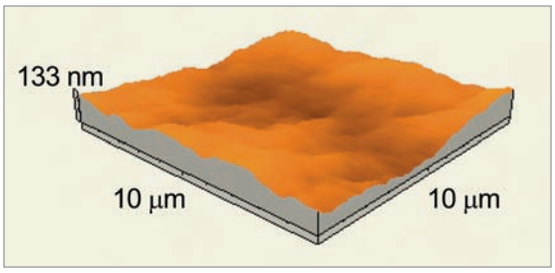

Fig. 9: AFM image of PIM (Ref.17).

SDCs of I^{-} ions and water in these membranes have been obtained by analyzing the experimentally measured exchange rate profiles of tritiated water (HTO) with H_2O and $^{131}I^{-}$ with $^{nat}I^{-}$ between the membrane and equilibrating solution using eq. 1.[17] The value of SDC(I^{-}) varies with nature and proportion of the plasticizer as well as its viscosity. The variation of D(I^{-}) as a function of Aliquat-336 shows a Aliquat-336 concentration threshold barrier in I^{-} ions diffusion that suggests minimum distance is required for hopping of a ion between adjacent exchange sites. The values SDC of water D(H_2O) in PIM samples has been found to be one order of magnitude higher than the value of D(I^{-}), indicating that water molecules diffuse independently across hydrophobic PIM, without being attached to diffusing counterions.

Conclusions

Radiotracers have been found to be ideal tool for studying the self-diffusion of counterions and water in the ion-exchange membranes. The interpretations of self-diffusion coefficients data reveal valuable information on different parameters influencing the diffusional-transport process. This has helped us in tuning properties of tailor-made polymer inclusion membranes and pore-filled membranes for a specific application.

Acknowledgements

Authors thank Dr. S. Sodaye, Dr. G. Suresh, Dr. Y.M. Scindia, Dr. Chhavi Aagarwal, Rakesh Kumar and Sanhita Chaudhury for their valuable contributions in the work described in this article.

References

1. Strathmann, H. "Ion-exchange membrane separation processes", *Membrane Science and Technology Series 9*, Elsevier, 2004, 1-20.
2. Sata, T. "Ion exchange membranes: Preparation, Characterization, Modification and Application", *The Royal Society of Chemistry*, Cambridge, 2004, 215-280.
3. Helfferich, F. "Ion Exchange ", McGraw-Hill, New York, 1962, Chapter 8.
4. Mauritz, K.A.; Moore, R. B. "State of understanding of Nafion", *Chem. Rev.* 104 (2004) 4535-4585.
5. Goswami, A.; Acharya, A.; Pandey, A.K. "Study of self-diffusion of monovalent and divalent cations in Nafion-117 ion-exchange membrane". *J. Phys. Chem. B* 105 (2001): 9196-9201; and references therein.
6. Yeager, H.L.; "Transport properties of perfluorosulfonate polymer membranes", in Eisenberg A. and Yeager H.L. (Eds.), *Perfluorinated Ionomer Membranes*, ACS Symp. Ser. No. 180, American Chemical Society, Washington DC, 1982, page no. 41-63.
7. Cranck, J. *The Mathematics of Diffusion*, 2nd ed.; Clarendon Press: Oxford, 1975.
8. Yasuda, H.; Lamaze, C. E.; Ikenberry, L. D. "Permeability of solute through hydrated polymer membranes, Part I, Diffusion of sodium chloride". *Macromol. Chem. 118* (1968): 19-35.
9. Suresh, G.; Sodaye, S.; Scindia, Y.M.; Pandey, A.K.; Goswami, A. "Study on physical and electrostatic interactions of counterions in poly(perfluorosulfonic) acid matrix: Characterization of diffusion properties of membrane using radiotracers". *Electrochimica Acta* 52 (2007): 5968-5974; and references therein.
10. Plesset, M. S.; Helfferich, F.; Franklin, J. N. *J. Chem. Phys.* 29 (1958):1064–1069.
11. Suresh, G.; Scindia, Y.M.; Pandey, A.K.; Goswami, A. "Isotopic and ion-exchange kinetics in the Nafion-117 membrane". *J. Phys. Chem. B* 108 (2004): 4104-4110.
12. Sodaye, S.; Suresh, G.; Pandey, A.K.; Goswami, A. "Inter-diffusion of exchanging counterions in poly(perfluorosulfonic) acid membrane". *J. Phys. Chem. B* 113 (2009): 12482–12488.
13. Krishna, R.; Paschek, D. "Separation of hydrocarbon mixtures using zeolite membranes: a modeling approach combining molecular simulations with the Maxwell–Stefan theory". *Sep. Purif. Technol.* 21 (2000): 111–136.
14. Sodaye, S.; Agarwal, C.; Goswami, A. "Study on multicomponent diffusion of ions in poly(perfluorosulfonated) ion-exchange membrane using radiotracers". *J. Membr. Sci.* 314 (2008): 221–225.
15. Chaudhury, S.; Agarwal, C.; Pandey, A.K.; Goswami, A. "Self-diffusion of ions in Nafion-117 membrane having mixed ionic composition", *J. Phys. Chem. B* 116 (2012): 1605"1611.
16. Agarwal, C.; Chaudhury, S.; Mhatre, A.; Goswami, A. "Anion Dependence of Transport of Mercury Ion through Nafion-117 Membrane". *J. Phys. Chem. B* 114 (2010): 4471–4476.
17. Kumar, R.; Pandey, A.K.; Sharma, M.K.; Panicker, L.V.; Sodaye, S.; Suresh, G.; Ramagiri, S.V.; Bellare, J.R.; Goswami, A. "Diffusional transport of ions in plasticized anion-exchange membranes". *J. Phys. Chem. B* 115 (2011): 5856–5867; and references therein.

Microwave Drilling of Materials

Shantanu Das
Reactor Control Division
and
Apurba Kumar Sharma
Department of Mechanical and Industrial Engineering,
Indian Institute of Technology, Roorkee, Uttarakhand.

Abstract

This is proof of principle of application of 'near-field microwave radiation', for material drilling. We report result of experiments conducted, for microwave-drilling of materials, using two types of setups, one-inside a domestic microwave oven and second -via co-axial cable applicator. Drilling with these techniques were carried out for wood, glass, aluminium, copper, mild-steel (MS), animal bones specimens.

Keywords: Microwaves, Drilling, Co-Axial applicator, Near Field, Monopole Antenna

Introduction

Microwaves are used to heat the materials like concrete, glass and ceramics and drill holes in them silently without creating dust. Microwave drilling would provide low cost solutions for these applications. In this article we report experimental results of 'microwave drilling of materials' a newly developed technique. This is the 'proof of principle' of application of 'near-field' microwave radiation, for material drilling.

Brief Theory of Microwave-drilling

The interaction of microwaves with materials can be classified into three categories. First the absorbing materials, with properties ranging from conductors to insulators which are having high dielectric loss and which absorb electromagnetic energy readily and convert it to heat. Second are the transparent materials, having low dielectric loss, such as glass, ceramics and air which allow microwaves to pass through easily with little attenuation. The third one is the opaque materials which are typically conducting materials with free electrons, such as metals, that reflect microwaves at room temperature, [1]-[4], [12]. For experimental works two different methods of microwave heating are generally used: direct microwave heating (DMH), and microwave hybrid heating (MHH) [1]-[4], [12]-[15]. For drilling we use DMH.

Material drilling by microwave is by process we call, 'locally induced thermal runaway', which is caused by an open ended co-axial applicator, (a monopole antenna Fig. 1). The microwave energy absorption, increases with increase of temperature; is the cause of local thermal runaway and formation of hot-spot resulting in local melting of material, evaporation, or forming liquid, gas or plasma respectively. This thermal runaway hot-spot formation and process of phase change is depicted in Fig. 4 as 'plasma' formation during the process of drilling with microwaves [13].

The dielectric loss factor $\varepsilon_r''(T)$; the imaginary part of complex dielectric function of the material $\varepsilon_r = \varepsilon_r' - j\varepsilon_r''$, is a function of temperature T. This factor tends to rise as temperature rises, hence greater amount of EM energy is dissipated (locally) as temperature rises,

giving further rise in local temperature. There is EM energy 'hogging' and further increase in temperature, giving rise to hot spot and induces thermal runaway.

Refer Fig. 1, (left) the M the magnetron 2.45 GHz 900W is the microwave source, the microwaves are launched to wave-launcher (WL) connected to a power co-axial cable of low loss, make BELDEN RG-213 (CO), via wave-guide (WR-340 type) to co-axial connector (RC). The other parts of the set-up are, control circuits, power circuits and cooling circuits. The figure-1 (right) gives the actual picture of the open ended co-axial cable (CO); and its extended 'tip' of 3.25 cm that is (about) quarter wavelength of 2.45 GHz microwave-source; which behaves as monopole antenna. Fig. 3 gives the photograph of actual set up, and the co-axial monopole which is kept inside an EM shield.

Assume perfect impedance matching then the entire watts of power delivered by the magnetron passes through the monopole to the antenna tip to the work-piece. The Electromagnetic (EM) radiation has a 'near field region' which is resonating in nature, followed by 'far field region' a travelling EM field in nature. The approximate distance to which we have resonating field is about a sixth of wave-length (that is about 2 cm from the antenna). The work piece is in the near field, and in resonating EM zone. Unlike the remote laser-based drill, the heat affected zone of near-field monopole drill bit is smaller, and for 2.45 GHz microwave, the molten region is typically less than 1 cm.

The same near field is also formed by a metal antenna which is kept at the centre of microwave oven, first acting as receiver, and then simultaneously transmitting its (absorbed) Electric field to the work-piece. The centre of oven has closed $\vec{H}$ field that induces $\vec{E}$ field at a conductor placed there. This scheme is shown in figure-2, a spring loaded drill bit (monopole antenna) held by concrete structure, and is kept inside microwave oven. In both the cases the work piece which is at the near field zone will be heated by $\vec{E}$ field (radiated by monopole). The monopole in both the cases acts as drill bit gets inserted to the work-piece.

We write standard EM-equation in frequency domain (1) and heat equation (2) in time domain; and these two are coupled-equations having two distinct time scales. The distinction between the time scales for EM wave propagation (1) and thermal diffusion (2) is ~Ins vs ~>ms respectively.

$$\nabla\times\left(\frac{1}{\mu_r}\nabla\times\vec{E}\right)-\left[\varepsilon_r'-\mathrm{j}\left(\varepsilon_r''+\frac{\sigma}{\omega\varepsilon_0}\right)\right]k_0^2\vec{E}=0 \qquad \mathrm{j}=\sqrt{-1} \quad (1)$$

$$\rho C_p\frac{\partial}{\partial t}T-\nabla\bullet\left(k_{th}\nabla T\right)=Q \quad (2)$$

Where $\vec{E}$ the electric field vector of the EM-field in the frequency domain, ω and k_0 are the angular-frequency ($\omega=2\pi f$; $f=2.45GHz$) and the free space wave number ($k_0=2\pi/\lambda_0$ with $\lambda\sim13\mathrm{cm}$). The work-piece is represented as μ_r, which is relative magnetic permeability, $\varepsilon_r=\varepsilon_r'-\mathrm{j}\varepsilon_r''$ the complex electric permittivity, and the electric conductivity σ. In (2), ρ is the local density of the work piece, C_p and k_{th} are the specific heat and thermal conductivity respectively; with T as slowly varying temperature. These material parameters of the work-piece ρ ,C_p ,k_{th} ,ε_r are considered as having known temperature (T) dependencies. The magnetic permeability of material in this X-Band of microwave radiation (2.45GHz) does not change much with temperature. The equation (1) and (2) are coupled by local EM heat source, and by the consequent variation of with temperature.

$$Q=\omega\varepsilon_0\varepsilon_r''(T)\frac{\left|\vec{E}\right|^2}{2} \quad (3)$$

The two time-scales of (1) and (2) as described earlier is also a cause of thermal runaway. The EM heat gets dissipated too quickly for thermal inertia system (2) to take it and conduct is away from the

local spot. Let δ_{hs} be the dimension of hot-spot, then we have, $\rho C_p \delta^2_{hs} / k_{th} \gg \tau$ where $\tau = 2\pi / \omega$ is period of the EM wave. This also quantifies time scale separation.

Microwave Drilling Experimental Setup

A method for drilling/cutting using microwave discharge was suggested in [1]-[4] but further studies were not reported. A novel method for drilling hard non-conductive materials by localized application of microwave energy was introduced in [5]-[7] [10]. We describe our two methods for experiments in microwave drilling experiment. The principle is same as of hot-spot formation with thermal runaway, described in section-2, [8] [9], [11]-[15] for non-metals as well as metals.

Setup for Drilling Inside Microwave Oven (Method-1)

The schematic diagram of the setup developed to perform microwave drilling inside a microwave oven is shown in Fig. 2. A spring of required stiffness was fixed to the bolt at the top of setup. The structure was made of concrete cement mix. The drill bit was fixed at the bottom end of the spring as shown in the schematic diagram (Fig. 2). The bit is working as microwave (monopole) antenna, receiving and transmitting. This entire set up is kept inside microwave oven. The work-piece is of metal sheets, or of insulator sheets. The metal sheets required susceptor material, (in our case charcoal powder) to initially couple the microwave onto metal, and increase its temperature locally; and thus initiate the thermal runaway process. The insulator work-pieces do not require the susceptor material. The procedure for non metals is same as that followed for metals. Here specimens were not covered to prevent reflection as non metals will not reflect microwaves. In this case susceptor was not needed.

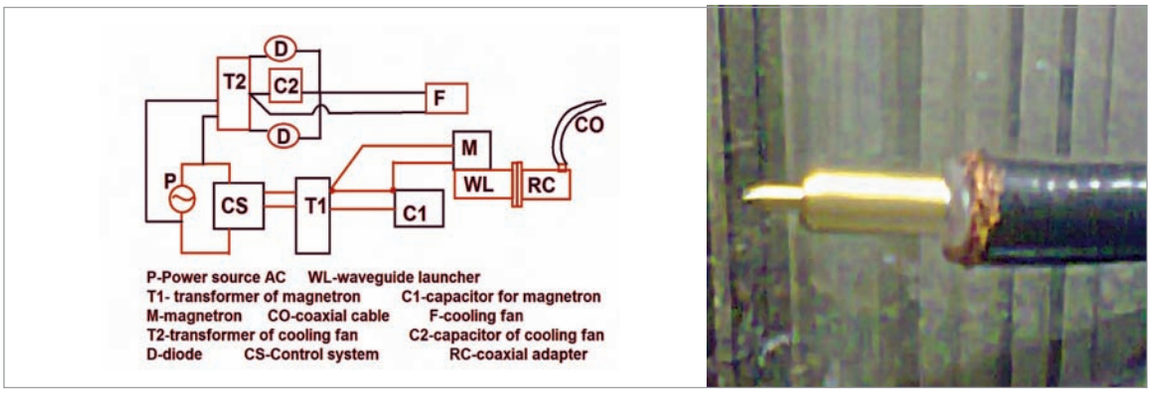

Fig. 1: Left the wave circuit of microwave drilling setup with co-axial applicator. Right is full view of open ended co-axial (CO) cable drill bit tip as monopole antenna

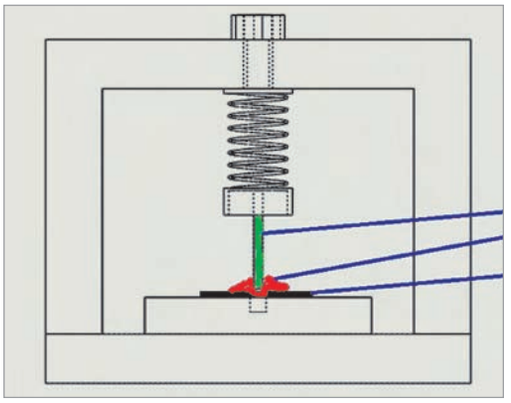

Fig. 2: Schematic diagram of microwave drilling setup for drilling inside oven

Table 1: Metal work-pieces

Material Drilled	Thickness of work-piece(mm)	Output power of microwave source	Time of exposure (s)	Drill bit feature (diameter in mm)
Aluminum 1	1	900 W	120	Tungsten bit (2mm)
Copper	0.5	900 W	150	Tungsten bit (2mm)
Mild steel	0.5	900 W	240	Tungsten bit (2mm)
Aluminum 2	1	900 W	60	SS bit (0.8mm)

Table 2: Non metal work-pieces

Material Drilled	Thickness (mm)	Power (W)	Time (s)
Borosilicate glass	1.5	360	8
Glass	8	500	4
Bone	6	500	12
Bone (wet)	6	500	15
Wood	2	500	5
Wood (wet)	2	500	5
Wood (wet)	5	700	10
Aluminum	1	700	5

Setup for Drilling with Co-Axial Applicator (Method-2)

The Fig. 3 describes the experimental set up. The coaxial cable of length 1m was fixed into the metallic box used as EM shield. The antenna 3.25 cm for co-axial applicator is in Fig. 1. We used different tips in our experiment (Table-1). Figure-4 gives the photograph of plasma formation while drilling process. This is observed in both the methods.

Observations

Aluminium specimen-1 was drilled with 2 mm Tungsten tool, which got melted and was burnt partially due to overexposure (120s); however a hole was formed. Similarly we drilled mild steel specimen

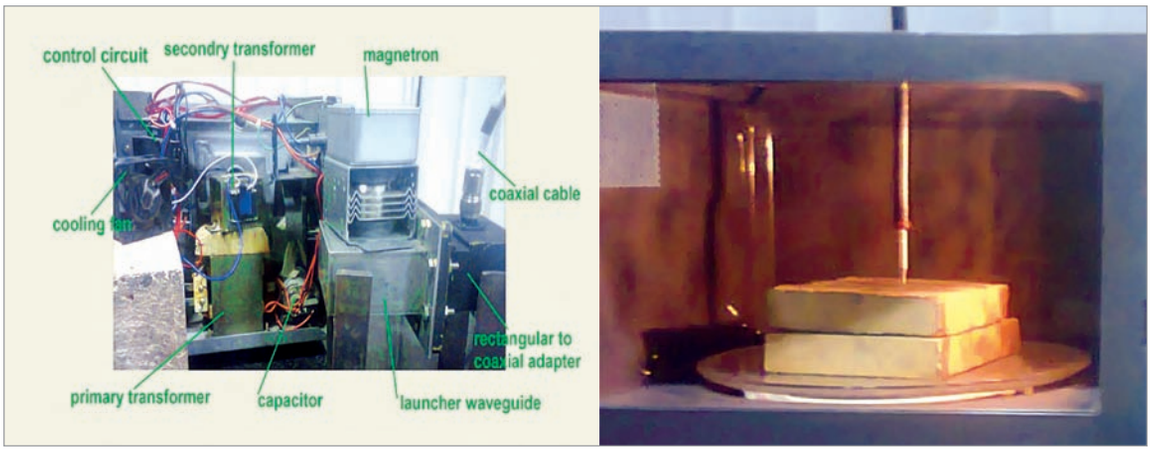

Fig. 3: Left photograph of the assembled setup to perform microwave drilling by microwave energy applied via co-axial applicator. Right photograph of the monopole antenna attached to the coaxial cable and put inside a chamber of EM shield tip is on the work-piece

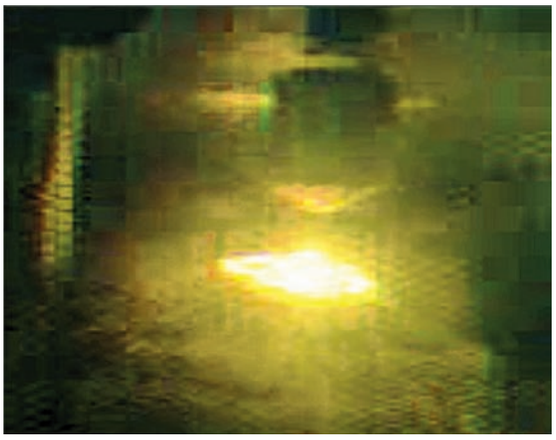

Fig. 4: Plasma formation while drilling glass inside oven

successfully .The photograph of the drilled copper strip 2mm hole is given in Fig. 5 (b). Aluminium specimen-2 was drilled with a stainless steel bit of 0.8 mm diameter and with 60 seconds exposure, which is shown in Fig. 5 (a). SEM image of the 0.8 mm hole drilled in Aluminium specimen-2 is given in; Fig. 6.

The Scanning electron microscope (SEM) photographs are taken in order to see if at all there is any kind of material transformation, due to application of microwave. Before drilling we have taken the SEM images of microstructure of the base metal. Later, after performing drilling operation, we have cut the specimen along the cross-sectional area, polished these specimen with emery paper and then etched the specimen (etching reagent varies for different material). After this standard process we again see the microstructure in SEM for details to view the specimen after drilling. For copper and MS; SEM show coarse graining near the drill hole that is due to slow cooling rate.

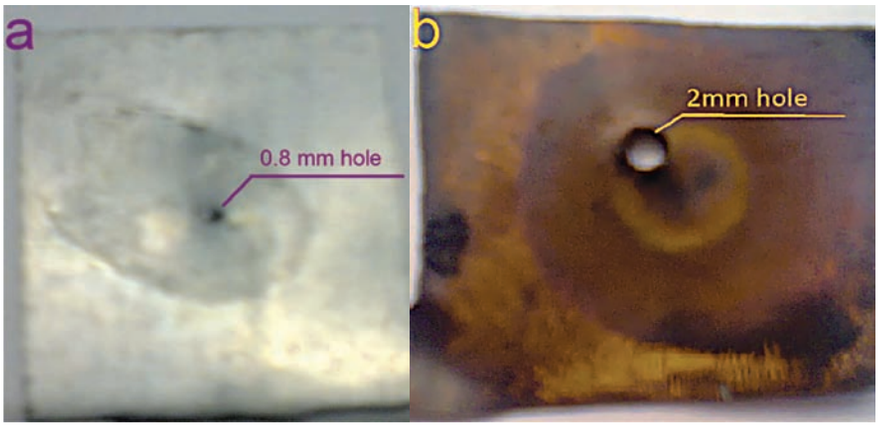

Fig. 5: (a) Aluminium with 0.8mm hole (b) Copper strip with 2 mm diameter hole

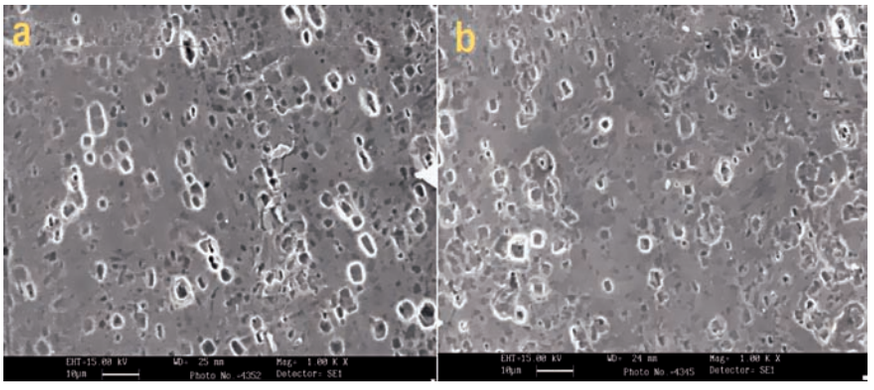

Fig. 6: SEM micrograph showing surface structure of Aluminium specimen (a) before microwave drilling (b) after microwave drilling

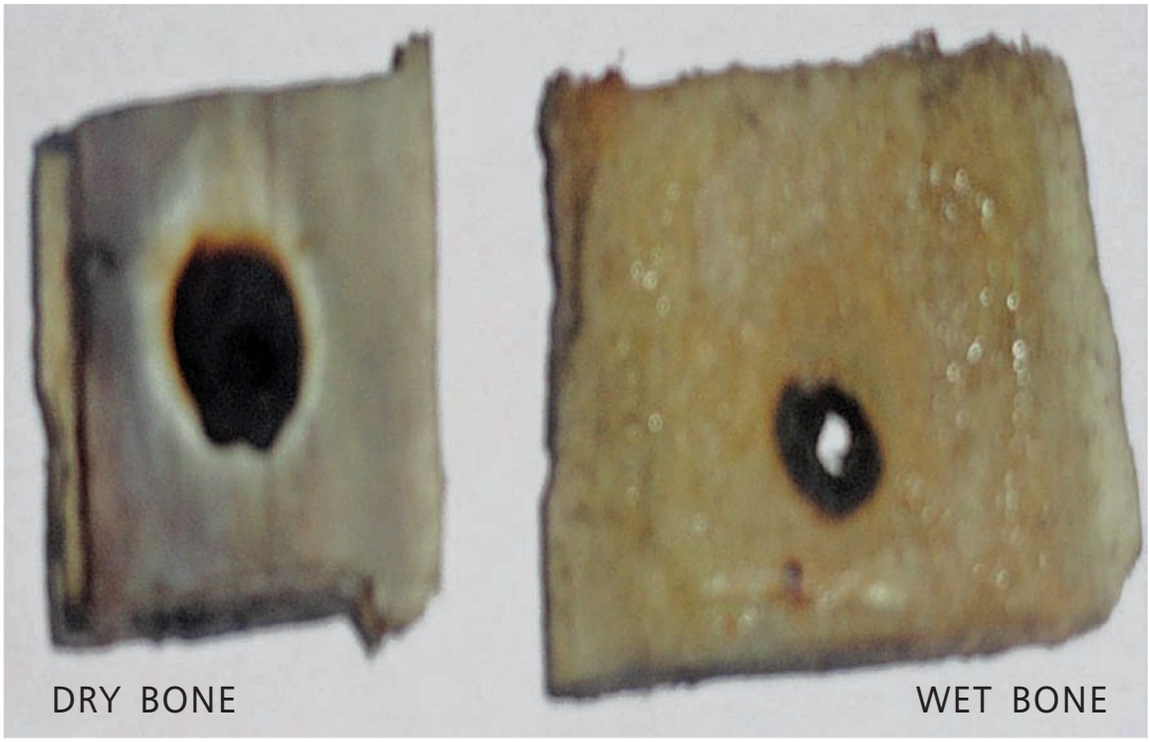

Fig. 7: Photograph of the hole drilled in bone without and with wetting

The drilling was done on glass wood bones; one such photograph of dry and wet bone drilled is shown in figure-7. Here we are not showing SEM photographs of all the drilled materials, a limited number are illustrated; wet specimens have lower carbonization.

Conclusions

Drilling for metals and non metals have been demonstrated via use of microwave radiation by prototype experimental set ups inside domestic oven and via co-axial applicator as proof of principle. SAMEER Govt. of India has shown keen interested in refining this prototype experiment for drilling with microwave, for professional usage for industry and medical applications. For future advancements, we plan to make solid state microwave drill system (for low power applications 10-100W) and set-up for high power up to 1200W; with co-axial 'wave-guide' applicator, tuning facility (3 Stub Tuner), circulator ports, metering for power transmitted and reflected, metering for temperature of hot-spot.

References

1. E.T. Thostenson, T.W. Chou, *Composites*: Part A 30 (1999)1055–1071.
2. David E. Clark, Diane C. Folz, Jon K. West, *Materials Science and Engineering* A287 (2000) 153–158.
3. H. S. Ku, E. Siores, A. Taube, Computers & Industrial engineering 42(2002) 281-290. Jiping Cheng, Rustum Roy, Dinesh Agrawal, *Mat Res Innovations* (2002) 5:170–177
4. S.P. Kozyrev, V.A. Nevrovsky, L.L. Sukhikh, V.A. Vasin, Yu. M. Yashnov, XVII International Symposium on Discharges and Electrical Insulation in Vacuum-Berkeley-1996
5. E. Jerby, V. Dikhtyar, 8th Ampere Proc., Bayreuth, Sept. 2001.
6. E. Jerby, V. Dikhtyar, O. Aktushev, Published in *Ceramic Bulletin* 82(2003) 35.
7. E. Jerby, V. Dikhtyar, O. Aktushev, U. Grosglick, www.sciencemag.org, Science Vol 298 18 October 2002

8. Titto John George, Apurbba Kumar Sharma, Pradeep Kumar et al, *Journal on Mechanical Engineering*, Vol. 2 No. 2 February - April 2012, pages 1-6.
9. Titto John George, Amit Bansal, Apurba Kumar Sharma, Pradeep Kumar et al, Proceedings of International Conference on Mechanical Engineering Technology, Kerala (ICOMET 2012), January 2012, pages 205-211
10. Eli Jerby, *J. Am. Ceram. Soc.*, 87 [2] 308–10 (2004).
11. Titto John George, Apurba Kumar Sharma, Pradeep Kumar, Rajesh Kumar, Shantanu Das, "Microwave Drilling: Future Possibilities and Challenges Based on Experimental Studies", International Conference on Emerging Trends in Manufacturing Technology Toc H Institute of Science & Technology Kerela, Sept, 5-6 , (2012).
12. Shantanu Das, Amit Bansal, Apurba Kumar Sharma, "Theory of Welding of Metallic Parts in Microwave Cavity Applicator", *Fundamental Journal of Modern Physics*-in press, 2012.
13. Shantanu Das, Rajesh Kumar, Prof. Apurba Kumar Sharma, Titto John George, Amit Bansal, "Phenomena of Electrostatic Resonance in Negative Permittivity Plasmoid in the Experimental Set Up for Microwave Near Field Applicator ", *Asian Journal of Physics Special Issue*-in press.
14. Apurba Kumar Sharma, Pradeep Kumar, R.S.Anand, Rajesh Kumar, Shantanu Das, "Material Processing with Microwave", BRNS-Project Sanction No.2010/36/60-BRNS/2048 dated 9-12-2010, (2009).
15. Shantanu Das, "RF Drilling of ceramics and rocks", High Precision Engineering VISION 2020, BARC, (2004)

Team for the project

Titto John George , Department of Mechanical Engineering, Viswajyothi College of Engineering and Technology Muvattupuzha, Kerala (Former IIT Roorkee ME student), Pradeep Kumar, Professor at Department of Mechanical and Industrial Engineering, I.I.T. Roorkee Amit Bansal, Research Scholar, Department of Mechanical and Industrial Engineering, I.I.T. Roorkee and Rajesh Kumar, Ion Accelerator Development Division IADD, BARC, Mumbai.

Table 2: Anti-inflammatory properties of plumbagin

	Activity	Method	Result	Reference
IN VITRO IMMUNOMODULATORY ACTIVITY OF PLUMBAGIN				
1.	Intracellular ROS levels	H_2DCF-DA fluorescence (spectrofluorimetry)	Plumbagin increased basal ROS levels in lymphocytes	(Checker et al. 2010)
2.	Intracellular GSH levels	Monochlorobimane fluorescence	Plumbagin depleted reduced thiols in lymphocytes	(Checker et al. 2010)
3.	Lymphocyte proliferation	Mitogen induced proliferation	Plumbagin inhibited mitogen lymphocyte proliferation in vitro	(Checker et al. 2009)
4.	Cell cycle progression	Propidium Iodide staining	Plumbagin inhibited Con A induced cell cycle progression in lymphocytes	(Checker et al. 2009)
5.	Cytokine secretion	ELISA	Plumbagin inhibited Con A induced IL-2, IL-4, IL-6 and IFN-γ cytokine secretion	(Checker et al. 2009)
6.	T cell activation	Flow cytometry	Plumbagin inhibited expression of Con A induced T cell activation markers CD69 and CD25	(Checker et al. 2009)
7.	Effect of anti-oxidants on immunosuppressive activity	Flow cytometry and ELISA	Thiol but not non-thiol anti-oxidants could abrogate the immunosuppressive effects of plumbagin	(Checker et al. 2010)
8.	Effect on activated lymphocytes	ELISA	Plumbagin inhibited cytokine production in activated lymphocytes	(Checker et al. 2010)
9.	Interaction with GSH	HPLC and LC-MS	Plumbagin reacted with GSH and formed plumbagin–GSH adduct	(Checker et al. 2010)
MECHANISM OF ACTION OF PLUMBAGIN				
10.	NF-κB activation	Western Blotting and EMSA	Plumbagin suppressed Con A induced IκBα degradation and NF-κB activation	(Checker et al. 2009)
11.	MAPKinase activation	Western Blotting	Plumbagin suppressed Con A induced phosphorylation of ERK but not P38, JNK or AKT	(Checker et al. 2010)
12.	S-glutathionylation	Immunoprecipitation	Plumbagin depleted free thiol groups on proteins and induced protein glutathionylation.	(Checker et al. 2010)
13.	JAK/STAT activation	Western Blotting	Plumbagin treatment inhibited both JAK1 and JAK2 as well as STAT1 and STAT4 phosphorylation	(Jia et al. 2011)
IN VIVO ANTI-INFLAMMATORY ACTIVITY OF PLUMBAGIN				
14.	Lymphocyte proliferation and cytokine secretion in vivo.	ELISA	Lymphocytes from plumbagin treated mice showed decreased responsiveness to Con A stimulation	(Checker et al. 2009)
15.	Graft-versus-Host Disease	Allogenic lymphocyte transfer	Treatment of lymphocytes with plumbagin prior to allogenic transplantation delayed the induction of GVHD in mice	(Checker et al. 2009)
16.	Collagen type II induced arthritis	Immunization with collagen and FCA	Plumbagin is effective in the mechanism based treatment of Rheumatoid arthritis	(Poosarla et al. 2011)
17.	Experimental Autoimmune Encephalomyelitis (EAE)	Mouse model of EAE	Plumbagin treatment ameliorated EAE	(Jia et al. 2011)
18	Human PBMC activation	Human PBMNC	Plumbagin inhibited PHA-induced cytokine production in human PBMC	(Kohli et al. 2010)

Development of an Inductively Coupled Plasma Mass-Spectrometer (ICPMS)

Rajendra Babu K., #Mishra J.K, Sandeep Choudary, Shinde K.R, Milind M.G, Joshi K.D, Kasbekar A.M, #Ramarao B.V., Nivedita Ved, Abichandani P.A., Ravisankar E., Gopalakrishna M., #Manjiri M. Pande, Saha T.K. and Nataraju V.

Technical Physics Division, #Ion Accelerator Development Division

Abstract

A Quadrupole based Inductively Coupled Plasma Mass Spectrometer (ICPMS) has been developed at Technical Physics Division, for the elemental determination at trace and ultra-trace levels and their isotope ratio measurements in various materials. The performance of the indigenously developed ICPMS has been tested for sensitivity, detection limits and linearity for different elements. The Sensitivity of the ICPMS was found to be 10-30 x10^6 cps/ppm, resulting in detection limits ranging from 10-50ppt, depending on the element of interest. Nuclear, Pharmaceutical and Biological samples were analyzed (to describe the operating characteristics and performance of the system).

Introduction

ICPMS is one of the most powerful techniques allowing multi-elemental detection over a wide linear dynamic range with very low detection limits, with isotopic ratio measurement capability [1-3]. It has been used for the determination of trace amounts of metals in a variety of samples. These include environmental samples, geological materials and biological samples. Laser ablation ICPMS became a powerful technique for both surface and bulk analysis of solids [4] and even for bio-imaging of tissues of nuclear workers and the ICPMS coupled to hyphenated techniques (e.g., Liquid Chromatography, gas Chromatography or Capillary Electrophoresis etc.) has immense applications in speciation analysis, proteomics, nano science and nuclear field [5-6] etc.

In this article, we describe, in detail, the ICPMS developed at Technical Physics Division, BARC. Its analytical capabilities and applications in various fields are also demonstrated, by analyzing samples from user Divisions.

Instrumentation

A schematic diagram of the ICPMS is shown in Fig.1 and Fig. 2 gives a photograph of the system. The system consists of different subsystems viz., a liquid sample introduction system, inductively coupled plasma torch (ICP) as an ion source, plasma sampling interface and ion optics for the extraction and focusing of the ions, a mass filter for mass analysis and detection and data acquisition system - all supported by electronics and vacuum systems. The individual components and operating conditions have been described in detail in Table 1.

Aqueous solutions are introduced into the inductively coupled plasma at an uptake rate of 0.3 mL/min by a concentric nebulizer and peltier-cooled spray chamber. The spray chamber is maintained at 4° C to reduce the solvent loading on the plasma and to reduce oxide interferences in the mass spectrum. The nebulized sample is ionized in the high temperature Argon plasma, which is generated in a Fassel type quartz torch by coupling a Radio frequency power to Argon gas using 2 ½ turn load

coil and 1700 W at 27.12 MHz from an RF Generator. The ions in the atmospheric plasma are extracted to ultra high vacuum for mass analysis using three stage differential pumping system; interface chamber (1st stage), Ion optics chamber (2nd stage) and mass analyzer- detector chamber (3rd stage).

The interface chamber consists of water cooled Nickel Sampler (1mm dia. aperture) and Nickel Skimmer (0.7mm dia. aperture). This interface region maintains 2 mbar pressure using a rotary pump (560 $Lmin^{-1}$). The ions from the skimmed plasma are extracted and focused in to the quadrupole mass spectrometer using double deflection ion optics system. The simulation of the ion optics is shown in Fig. 3. This ion optics prevents the neutrals and photons from reaching the detector and hence reduces the background noise. This region maintains pressure of $8x10^{-4}$ mbar and is pumped by 665 Ls^{-1} Turbo molecular pump.

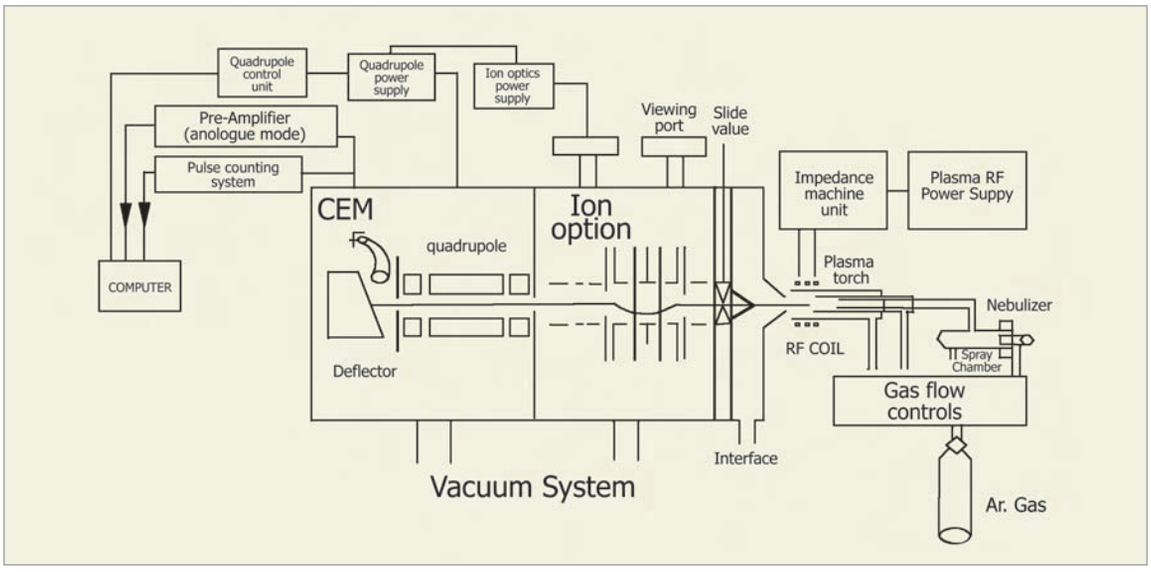

Fig.1. Schematic of ICPMS

Fig.2. Photograph of ICPMS

Table 1: Instrumental components

Component Manufacturer/Description	Operating conditions
Sample Introduction system:	
✓ Concentric Nebulizer (Model:AR35-1-FC1E,Glass-Expansion)	Sample uptake rate= 0.3 mL min^{-1}
✓ Peltier cooled Spray chamber (Model: KT-1023, Glass Expansion)	Spray chamber temperature: 4°C
✓ Peristaltic Pump (Minipuls 3, Gilson)	
ICP torch and RF generator:	Argon gas flow rates
✓ Fassel type torch (Model:30-808-0234, Glass Expansion)	Plasma gas: 16 L min^{-1}
✓ RF coil (2 ½ turn copper coil, TPD/BARC)	Auxiliary gas: 0.8 L min^{-1}
✓ RF generator (27.12MHz;power=1700 W with auto impedance matching network, TPD/BARC)	Carrier gas : 1.05 L min^{-1}
	Forward power: 1350 W
	Reflected power <10 W
Ion extraction interface:	Sampling depth: 8mm
✓ Nickel Sampler cone (Model: VG-1001-Ni)	Sampler orifice diameter: 1 mm
✓ Nickel Skimmer cone (Model: VG-1004-Ni)	Skimmer orifice diameter : 0.7 mm
	Sampler skimmer separation :7 mm
Vacuum system:	
Three stage differentially pumped system	1^{st} stage pressure:2 mbar (measured by Pirani Gauge TPR 280)
✓ 1^{st} stage was pumped by a rotary pump (model: Penta 35, pumping speed 560 $Lmin^{-1}$)	2^{nd} stage pressure:$8x10^{-4}$ mbar (measured by Full Range Gauge PKR 251)
✓ 2^{nd} stage was pumped by a Turbo drag pump (model: HiPace700, pumping speed 665 Ls^{-1})	3^{rd} stage pressure:$2x10^{-6}$ mbar (measured by FullRange Gauge PKR 251)
✓ 3^{rd} stage was pumped by a Turbo drag pump (model: Hipace300, pumping speed 255 Ls^{-1})	
✓ Backup for both TMPs : A rotary pump (model: DUO10M, pumping speed 330 $Lmin^{-1}$)	Back up pressure: $5x10^{-2}$mbar (measured by Pirani Gauge TPR 280)
Ion optics:	Extractor=-400V;
✓ Double deflection ion optics with Einzel lens	Focus= -20V; Bias= -150V;
	Deflector1&3=175V;
Mass Analyzer:	Deflector2=25V; Einzel lens1&3=-10v; einzel lens2=0V
✓ Quadrupole mass analyzer with pre filters	
✓ Rod diameter : 16mm	Pole bias :10V
✓ Rod length : 225mm	Unit mass resolution throughout the mass range
✓ Mass range: 6-260amu	
✓ Quadrupole RF : 1.2MHz;100W	
Detector	SEM HV: -1500V (in Analog mode)
✓ Secondary electron multiplier (Model:14562A; ETP make)	SEM HV: -3000V (in pulse mode)
Data acquisition	
✓ Multi-Function card (TPD/BARC make)	
✓ Lab view based software	

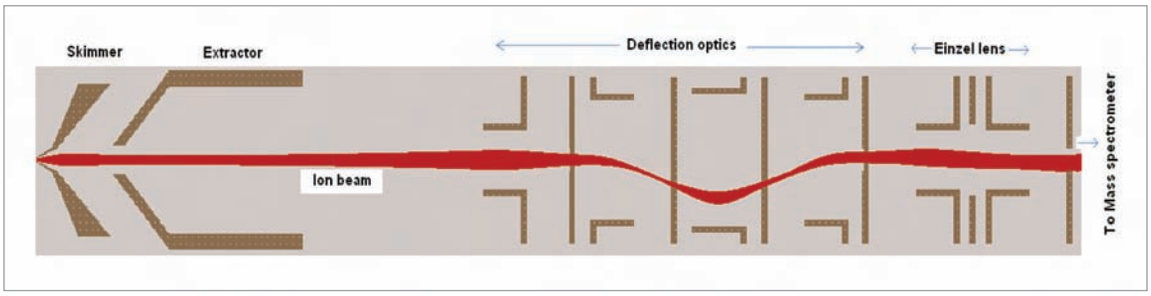

Fig.3. Simulation of Ion Optics

Quadrupole mass analyzer with pre-filters is used to separate the ions according to their mass. It consists of four stainless steel rods of 16 mm diameter and 225 mm length. The mass range of system is 6-260 amu at quadrupole RF frequency of 1.2 MHz. Unit mass resolution can be achieved throughout the mass range. The mass analyzed ions are detected by a secondary electron multiplier (SEM), which can be operated in both analog and pulse counting modes. This region maintains a pressure of $2x10^{-6}$ mbar and is pumped by 255 Ls^{-1} Turbo molecular pump. The signals from the SEM are processed and displayed by a FPGA based multi-function card and a Labview-based software.

Analytical Performance:

A typical mass spectrum of a mixture of rare earth elements is shown in Figure 4.

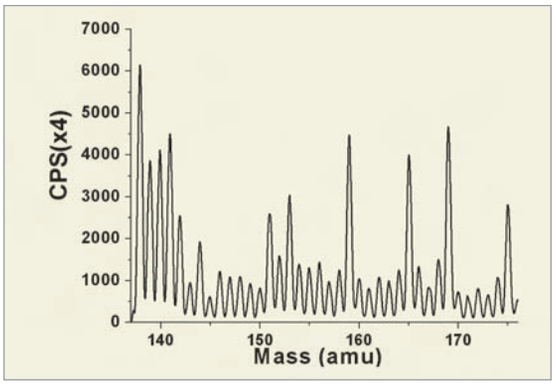

Fig.4. Typical Mass Spectrum

Individual solutions of boron, cobalt, silver, cadmium, cerium and uranium in the concentration range of 10 ppb to 100 ppb are prepared from NIST standards. The instrument is tuned for optimum sensitivity for each element before measurement.

The linearity of the instrument is shown in Fig. 5. The figure shows the linear performance of the instrument with a regression value > 0.999 for different elements. The sensitivity of the ICPMS was found to be $10\text{-}30x10^{6}$ counts per second (cps) per ppm, resulting in the detection limits ranging from 10-50 ppt depending on the element, which is shown in table 2. The sensitivity of the instrument for different elements is shown Fig.6.

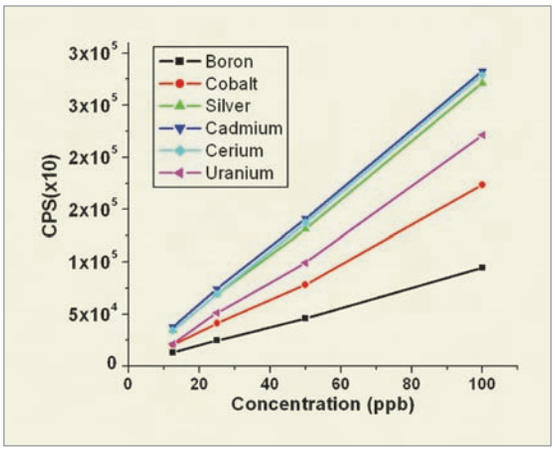

Fig.5. Linearity for B, Co, Ag, Cd, Ce and U

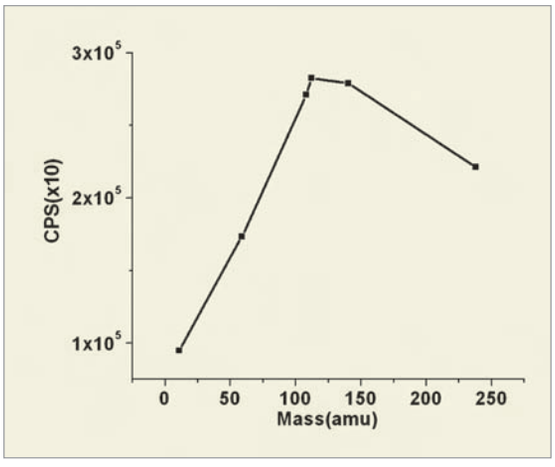

Fig.6. Mass Response of the system

Table 2 : Detection Limits of the system

S.No	Element	Sensitivity [CPS(x10)/100ppb]	Instrument Detection limits (3σ) (ppt)
1	^{11}B	75822	98.9
2	^{59}Co	173565	17.2
3	^{107}Ag	140613	21.3
4	^{114}Cd	81231.	36.9
5	^{140}Ce	246802	12.1
6	^{238}U	219742	13.6

Applications:

i) Determination of impurities in Trichlorosilane:

The most common method of producing high-purity polycrystalline silicon uses trichlorosilane as a raw material. Polycrystalline silicon, also called polysilicon, is a material consisting of small silicon crystals. It is used in making electronic components and solar cells. After distilling trichlorosilane, the residue left was analysed for various elements. Typical results are given in Table 3.

Table 3: Impurities in Trichlorosilane

Elements	Sample 1	Sample 2
	ng mL^{-1}	ng mL^{-1}
Mn	28.5±1.5	275.8±9.0
Mo	1.0±0.1	8.1±0.5
Cu	252.0±10.0	381.6±11.0
Ni	632.6±15.0	1023.8±20.0
Co	19.8±1.2	32.0±1.6
Ga	46.0±2.3	49.2±2.0
As	<2.0	<2.0
In	<1.0	2.8±0.2
Mg	51.3±2.0	114.5±4.2
	µg/ml	µg/ml
B	10.0±0.5	38.3±1.5
Fe	1.7±0.1	12.4±0.8

ii) Determination of Pd and Rh in Pharmaceutical sample:

Pd and Rh are used as catalysts during the manufacture of drugs. Hence, as a part of quality checks the drug was analyzed for Pd and Rh at m/e values of 108 and 103 respectively. Concentration values of Pd were found to be less than 100 ng g^{-1} and the values for Rh were found to be less than 70 ng g^{-1}.

iii) Determination of Thorium-232 in Human Liver Cells (HepG2):

The study of qualitative and quantitative interaction of ^{232}Th with human liver cells (HepG2) was carried out by using ICPMS. Results showed that the total cell bound thorium was ~100 fold higher than in culture medium (Fig. 7a & 7b). However, when the thorium treated cells were harvested with trypsin-EDTA, cell bound thorium was found ~25 folds lower than in cells harvested without using trypsin-EDTA.

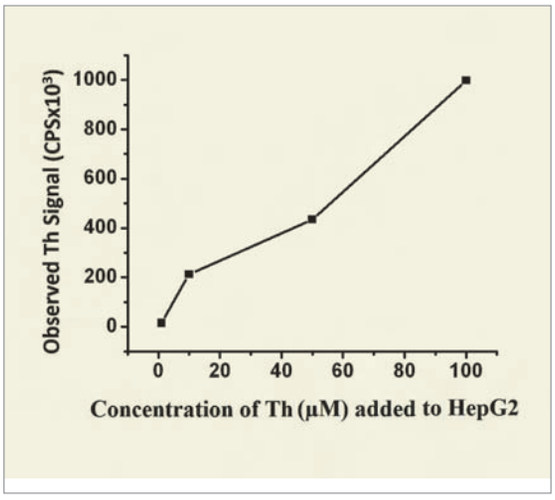

Fig.7a.: Observed ^{232}Th signal in human liver cells harvested without trypsin-EDTA

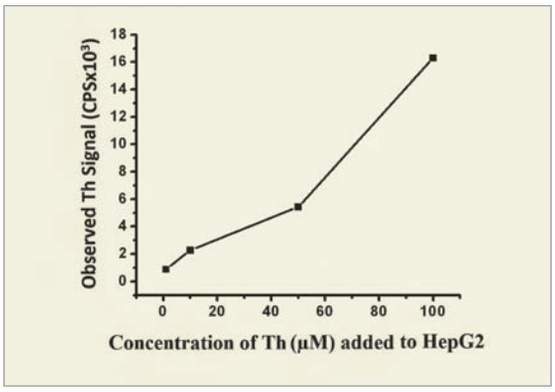

Fig.7b.: Observed ^{232}Th signal in cell culture medium

iv) Boron Isotope Ratio analysis:

Boron samples of different ^{10}B enrichments were analyzed for the ^{10}B/ ^{11}B isotope ratios to access the instrument mass bias and contribution of ^{12}C signal on ^{11}B signal. The accuracy of the ^{10}B/ ^{11}B isotope ratios is within ± 3% of true value, which was confirmed by Thermal ionization mass spectrometers. The results are shown in Table 4.

Conclusions:

A Quadrupole based ICPMS has been fabricated and tested for trace elemental and isotope ratio determination in various materials. The performance of the spectrometer has been tested extensively by recording the mass spectra for the determination of sensitivity, detection limits and linearity of the response and also isotope ratio measurements for some elements. Further, the spectrometer has been used for different applications to determine elemental concentrations in nuclear biological and pharmaceutical samples.

Acknowledgements:

The authors gratefully acknowledge the contributions and motivation by Shri V.K. Handu, Ex. Head, TPD and staff members of Mechanical design and Assembly Section, Advanced Electronics & Instrumentation, Digital Controls Sections of TPD and others who greatly assisted in the development of the project. They are greatly indebted to Dr.S.K. Gupta, Head, TPD, for his constant encouragement. They also express sincere thanks to all user departments for their constructive feedback, which encouraged the team to improve the designs for better performance and reliability.

References:

1. R.S. Houk, *Acc. Chem. Res.*, 27 (1994): 333-339
2. A. Montaser, *Inductively Coupled Plasma Mass Spectrometry*, *VCH, New York*, 1996
3. G.M. Hieftje, L.A.Norman, *Int. J. Mass Spectrom. Ion Processes*, 519 (1992): 118-119
4. Joachim Koch, D.Gunther, *Applied Spectroscopy*, 65 (2011): 155A-162A
5. R. Henry, D. Koller, D.W. Koppenaal, J. Wacker, *J. Radioanal. Nucl. Chem.* 249 (2001): 103–108.
6. I. Guenther-Leopold, J.K. Waldis, B. Wernli, Z. Kopajtic, *Int. J. Mass Spectrom.* 242 (2005):197–202.

Table 4 : Inter-comparison study

Sample	% of ^{10}B ICPMS (TPD)	% of ^{10}B TIMS (TPD)	% of ^{10}B Commercial TIMS
Bottom1	39.65	39.93	40.20
Bottom2	45.17	44.93	45.10
Bottom3	42.00	41.27	41.34
Bottom4	89.70	86.80	86.90

Indigenous Development of High-resolution Atomic Beam Fluorescence Spectroscopy Facility for Precision Measurements of Isotope Shifts and Hyperfine Structure

G.V.S.G. Acharyulu, M.Sankari, P.V. Kiran Kumar, M.V. Suryanarayana and T. Mukherjee
National Centre for Compositional Characterisation of Materials, Chemistry Group

Abstract

A compact and versatile ultra-high vacuum chamber in combination with a resistively heated graphite tube atomic beam apparatus for sub-Doppler fluorescence experiments has been designed and developed. The spectral resolution achieved in the developed system is more than adequate to clearly observe all the sub-Doppler hyperfine features in the D2 spectrum of rubidium. The compact interaction geometry, flexibility in changing the atomic beam source and simplicity of the entire set up makes it useful for the measurement of isotope shifts and hyperfine structure with a precision of $<$100 kHz.

The developed system is versatile enough and can be adopted to carry out high resolution atomic fluorescence experiments on radio-active isotopes after making minor modifications to ensure radiation safety. The spectral resolution and small sample size requirement would enable accurate measurements of nuclear parameters such as nuclear size, deformation, magnetic moments, quadrupole moments, spins etc. This finds applications in AVLIS and ADSS programmes.

Keywords: Atomic beam fluorescence, laser spectroscopy, isotope shift, hyperfine structure, sub-Doppler spectroscopy, laser isotope separation, radioactivity, AVLIS, ADSS, nuclear structure

Introduction

High-resolution optical spectroscopy has been used to determine isotope shifts and hyperfine structure for large number of isotopes, both stable and unstable, and this has led to valuable information about nuclear properties such as spin, magnetic moments, nuclear charge radii and nuclear shape. Measurement of isotope shifts and hyperfine structures of an isotopic chain is of interest for departmental applications. For example, measurement of isotope shift between ^{235}U - ^{238}U, ^{232}U - ^{233}U along with oscillator strength information of various transitions allow one to arrive at appropriate photoionization schemes for AVLIS [1-2]. Considering its importance, continuous efforts are being made to record emission spectrum of ^{232}U –^{238}U for deriving isotope shifts [3].

Measurement of isotope shifts of stable isotopes; unstable / radioactive nuclides of an isotope chain provide information on nuclear size, shape and spin. Such laboratories already exist worldwide in countries like Russia (FLNR), Korea (KAERI), Germany (GSI), TRIUMF (Canada), Finland (*University of Jyvaskyla*) to name a few.

In the Indian scenario, and more particularly in DAE context, the requirement of the nuclear data of various target materials (^{209}Bi, ^{208}Pb, ^{207}Pb, ^{206}Pb, ^{204}Pb, ^{186}W, ^{184}W, ^{183}W, ^{182}W, ^{181}Ta, Zr, Sn, Hg, U, Pu, F, Cl, Na, Fe, Al), minor actinides (^{237}Np, ^{238}Np, ^{241}Am, ^{242m}Am, ^{242}Am, ^{243}Am, ^{242}Cm, ^{243}Cm, ^{244}Cm, ^{245}Cm,

^{246}Cm, ^{248}Cm), long lived fission products, fuel materials, structural and shielding materials used for ADSS is very essential and is also well realized [4].Measurement of isotope shifts using high precision laser spectroscopy is an excellent technique for the determination of few nuclear properties.

In fact, recently, the radius of the proton was re-measured using Lamb shift measurement of muonic hydrogen and it has been reported that the proton radius is 0.84184(67)fm (which is 4% smaller than the CODATA value of 0.8768(69)fm. This is the most accurate proton size measurement ever done [5].

High precision 2s $^2S_{1/2}$ – 3s $^2S_{1/2}$ Doppler-free two photon spectroscopy of natural (^{6}Li and ^{7}Li) and radioactive (^{8}Li, ^{9}Li and ^{11}Li) has shown that the nuclear charge radii decreases continuously from ^{6}Li to ^{9}Li, while a sudden increase in the nuclear size is observed in case of ^{11}Li resulting in the formation of "^{11}Li halo nuclei" [6]. The above examples illustrate the ability of precision laser spectroscopy methods for deducing certain nuclear parameters.

Resonance fluorescence of atoms in an atomic beam allows one to precisely measure hyperfine splitting and isotope shift with high accuracy. The resolution and sensitivity of the atomic spectra depends on the laser parameters (frequency jitter, drift, power), atomic beam parameters (atomic beam diameter, mean free path, degree of collimation, Doppler shift, background radiation from source) and detection parameters (fluorescence spot size, signal collection efficiency, signal to noise ratio) etc [7,8].

The salient features of the atomic beam fluorescence setup developed at CCCM, Hyderabad, have been described briefly in the current article, addressing all the issues mentioned above.

System description

CCCM has procured cw ring dye laser and cwTi:Sapphire laser systems under the Xth plan project as part of RIMS programme. The lasers have a frequency jitter of $<$ 50kHz when they are actively locked to the temperature stabilized reference cavity. The high resolution lasers can be tuned over a wide spectral range for carrying out isotope shift and hyperfine structure measurements of isotopes of several elements.

Usually the dominant contribution to the atomic spectral width is from Doppler broadening, which often limits the resolution. However, in order to measure isotopes shifts and hyperfine structures of constituent isotopes for a given transition of an element, it necessary to employ sub-Doppler or Doppler-free high resolution laser spectroscopy techniques. To overcome the limitation set by Doppler broadening, primarily three techniques are used: a) the crossed-beam method; b) saturation absorption spectroscopy; and c) the two-photon spectroscopy. However, crossed-beam method is more versatile and allows one to record sub-Doppler spectrum with very small laser powers (in mW levels). In this technique, the laser beam intersects the atomic beam at right angles. A narrow vertical slit collimates the atomic beam to give a small angular spread. Collimation reduces the Doppler broadening by a factor determined by the angular spread. This technique allows one to unambiguously resolve and identify all hyperfine components of odd isotopes which enables precise measurements of isotope shifts and the hyperfine structure constants.

Development of sub-Doppler high resolution laser atomic beam fluorescence spectroscopy technique requires development and integration of a suitable atomic beam source, interaction chamber and fluorescence detection. A high-resolution atomic beam fluorescence spectroscopy facility has been designed and developed (Fig. 1). A resistively heated graphite tube atomic beam source with a collimation ratio of ~20 was designed, tested and integrated into a compact interaction chamber for atomic beam fluorescence experiments (Fig. 2). The laser-atom interaction chamber and the source have been designed so as to achieve sub-Doppler resolution. The source chamber and the interaction chamber

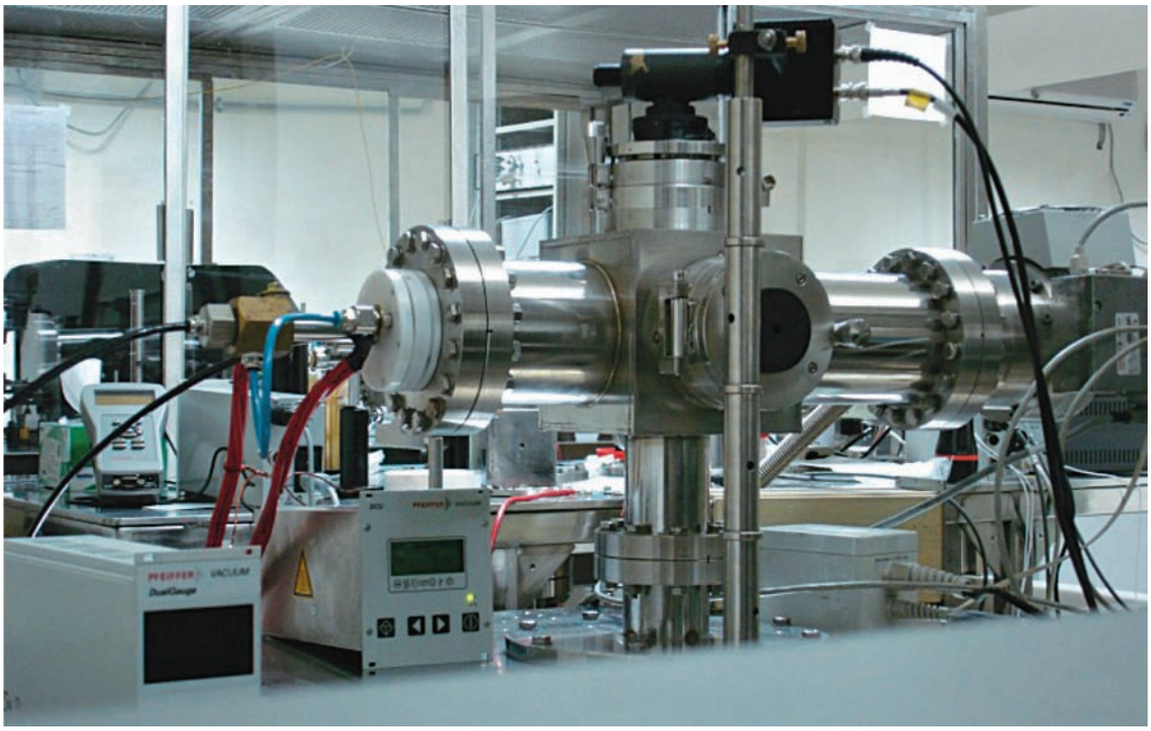

Fig. 1: A photograph of the atomic beam fluorescence spectrometer developed for precision measurements of isotope shifts and hyperfine structure.

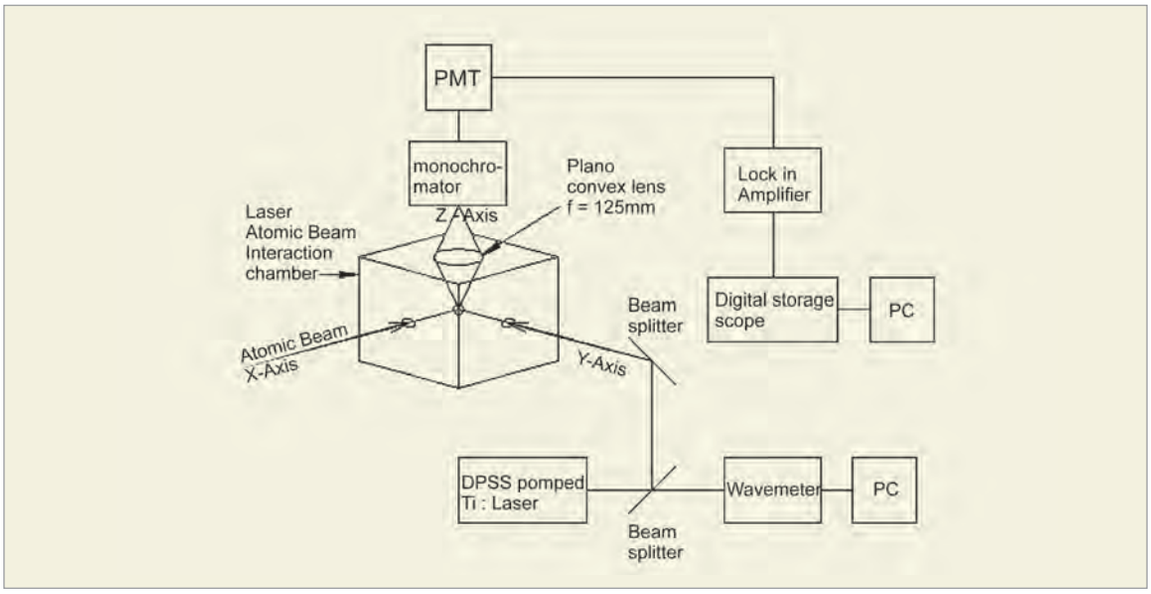

Fig. 2: Schematic of the experimental set-up in LEAFS with the laser-atomic beam interaction in the XY plane and detection of the fluorescence photons in the Z-axis.

are connected by a long tube which forms one of the six ports of the cuboidal chamber. This tube houses a collimator block. This collimator block additionally functions to establish a differential pumping between the source and the interaction chamber. A series of light baffles are used for minimizing the background radiation from atomic beam source. Additionally a light baffle comprising of graphite pipe has been inserted perpendicular to the atomic beam axis at the interaction region which

further minimizes the back ground radiation from the source. Atomic beam interacts with the laser orthogonally to reduce the Doppler broadening. The incident laser beam is retro-reflected into the laser axis to eliminate the Doppler shifts due to residual angle (due to misalignment) between atomic beam and the laser. This ensures that the fluorescence peak lies within 100 kHz of the resonance center. Due to the elimination of systematic shifts, hyperfine splittings and isotope shifts could be measured with high accuracy.

The advantage of the source is that it requires very small amounts of sample (few mg) for achieving high signal to noise ratio (>1000).The compact size of the source makes the turn-on and the turn – off times relatively less in comparison to the number of hours of operation of the atomic beam. The turnaround time is typically about 2 hours.

Experimental

Light resonant with the atomic transition was generated by a DPSS pumped cw-ring Ti: Sapphire laser having a frequency jitter of <50 kHz. A small fraction of the laser light is fed to a wavemeter with a resolution of 30 MHz to monitor the laser wavelength. The wavemeter is calibrated using a stabilized reference laser (frequency-stabilized He-Ne laser). The resonance fluorescence was collected using a Czerny Turner monochromator. This monochromator minimizes the amount of stray light reaching the photomultiplier tube and thus the S/N ratio of the fluorescence signal is significantly improved. The atomic hyperfine spectrum was recorded using a digital storage oscilloscope. The dimension of the fluorescence spot has been imaged through the view port and is found to be~ 3mm x 6mm.

High resolution sub-Doppler spectroscopy of Rubidium and Potassium isotopes:

a) Rubidium

To evaluate the spectral resolution and sensitivity of the developed system, experiments have been carried out on Rubidium and potassium atomic beam. The atomic beam of rubidium and potassium is produced by thermal evaporation of a mixture of rubidium chloride and potassium nitrate placed in a graphite crucible. Due to the resistive heating, the oven heats up to temperatures of about 1000 K. At this temperature a sufficiently dense atomic beam of Rb is produced. The atomic density is estimated to be ~10^{10} atoms/cm^3 while diameter of the atomic beem is ~10mm. The atoms leave the oven through a small hole of 2.0 mm diameter. The laser light from a DPSS pumped Ti:Sa laser intersected the atomic beam orthogonally at about 20 cm downstream

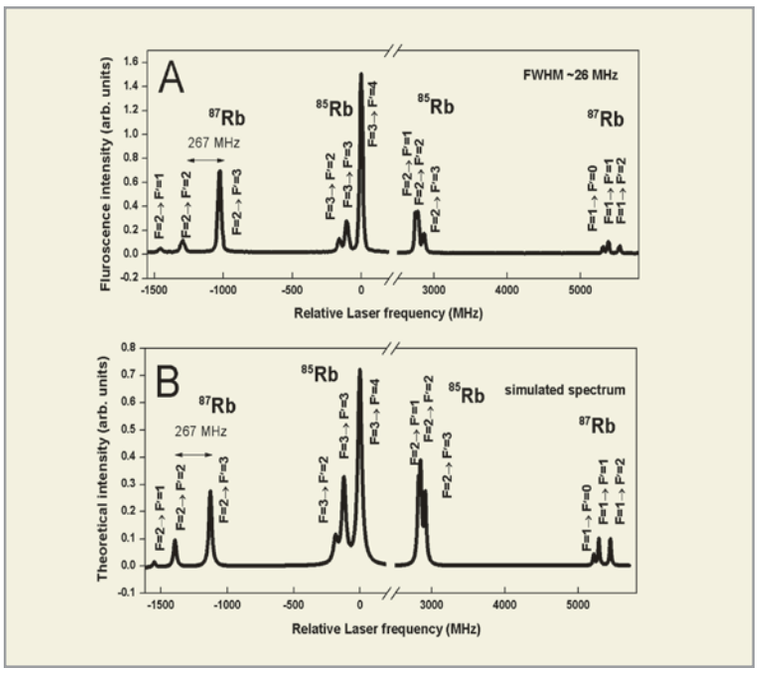

Fig. 3: Experimental (A) as well as the theoretical (B) laser induced fluorescence spectrum for the $5^2S_{1/2}$ – $5^2P_{3/2}$ D2 transition of rubidium spanning the entire range covering the hyperfine spectrum of ^{87}Rb and the ^{85}Rb isotopes. The sub-Doppler peaks of both the isotopes are seen whose FWHM is ~ 26 MHz.

from the oven. The background pressure in the vacuum system was about 5×10^{-7} mbar. Thefluorescence light is imaged on to a low resolution monochromator and is detected using a photomultiplier tube (PMT) which is placed above the intersection region of atomic beam and laser beam. The detected laser induced fluorescence for $5^2S_{1/2} - 5^2P_{3/2}$ D2 transition of Rubidium is shown in Fig. 3A. Atomic beam fluorescence spectrum for the entire range of the ^{87}Rb and the ^{85}Rb isotopes has been recorded. The theoretical spectrum has also been simulated for comparison with the recorded spectrum (Fig.3B). The best spectral resolution that could be achieved after optimizing

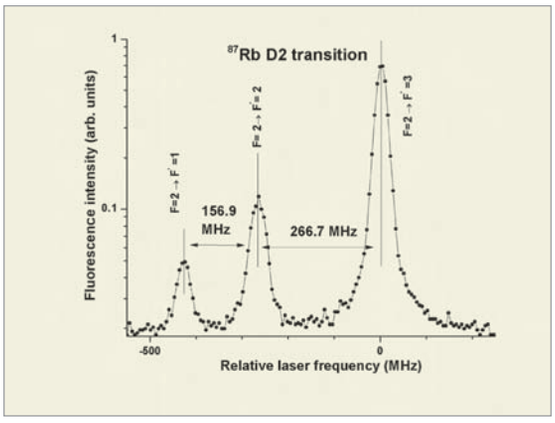

Fig. 4: The hyperfine spectrum of the ^{87}Rb isotope for the $5^2S_{1/2} - 5^2P_{3/2}$ D2 transition. The FWHM of the transition is observed to be ~ 16 MHz.

the power was ~16 MHz (Fig. 4) and is limited by the angular spread of the collimator.

The experimental design and conditions for the production of collision free atomic beam have been optimized and the spectral resolution achieved clearly establishes the observation of all the hyperfine components of both the Rb isotopes.

b) Potassium

Laser induced fluorescence from atomic beam of potassium has also been recorded. The laser was operated at a power of 23 μW and the temperature of the atomizer was maintained at ~950 K for obtaining sufficient density of atomic beam. Unlike the frequency separation between the hyperfine components of D2 transition of Rb, the hyperfine separation between the components of K isotopes is much smaller (30 – 55 MHz).The entire fluorescence spectrum of $4^2S_{1/2} - 4^2P_{1/2}$D1 transition of the ^{39}K and ^{41}K isotope has been recorded in two different frequency ranges.

Adjacent hyperfine components of the ^{41}K isotope could not be resolved (Fig.5) due to very small separation between the hyperfine components (~ 30 MHz). To completely resolve the components, the spectral resolution needs to be further improved; however, it can be done only at the cost of sensitivity. The hyperfine components of the ^{39}K isotope could

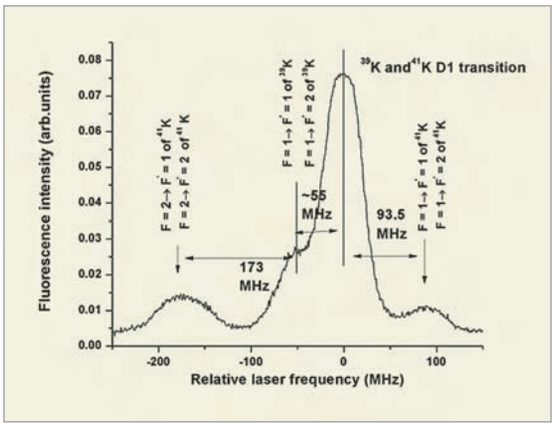

Fig. 5: The hyperfine spectrum of potassium isotopes for the $4^2S_{1/2}$ - $5^2P_{1/2}$D1 transition recorded for a laser power of 23 μW.

be partially resolved (Fig.5) due to relatively larger separation (~ 55 MHz).

The hyperfine components of the major ^{39}K isotope originating from the lower F=2 hyperfine level have been shown in Fig.6. As it can be seen in the Fig.6, the hyperfine components, having similar intensities and frequency separation of ~ 55.5 MHz could be resolved partially. This clearly shows the limit of the resolution of the system in the present configuration.

It is possible to improve the resolution further by the control of angular spread of the atomic beam. Minor design modifications can be made on the system such as type of atomizer required, degree of

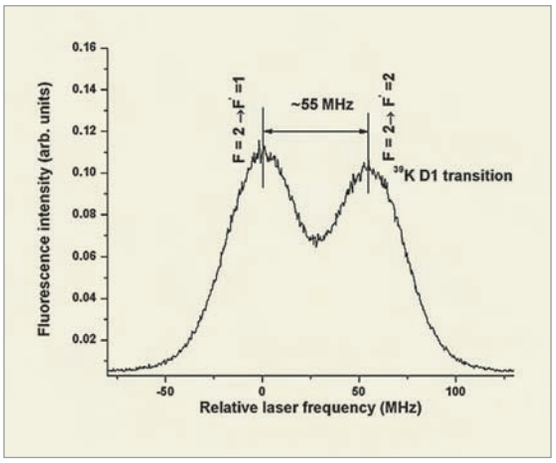

Fig. 6: The sub-Doppler peaks for the ^{39}K isotope for the 4 $^2S_{1/2}$ - 5 $^2P_{1/2}$D1 transition which has been recorded for a laser power of 23 μW.

resolution desired etc on case by case basis and this would enable one to carry out precision isotope shift and hyperfine structure measurements on most of the isotopes relevant to the department.

Conclusions

We have developed a high-resolution atomic beam fluorescence spectroscopy facility for precision measurement of isotope shifts and hyperfine structure. We have achieved a spectral resolution of ~16 MHz for the 5 $^2S_{1/2}$ – 5 $^2P_{3/2}$Rubidium D2 transition. We have also recorded the sub-Doppler spectrum of the $4^2S_{1/2}$– $5^2P_{1/2}$ D1 transition of potassium for the ^{39}K and ^{41}K isotopes and measured the hyperfine splittings.

The setup can be readily adopted for measurements on radioisotopes with adequate radiation safety measures, which can find applications in AVLIS and experiments to derive nuclear data of short lived isotopes relevant to ADSS program.

References

1. P. RamakoteswaraRao, "Laser isotope separation of uranium", *Current Science,* 85, 615 – 633 (2003).
2. Yu.P. Gangrsky, B.K. Kul'djanov, K.P. Marinova, B.N. Markov, S.G. Zemlyanoi, "Hyperfine anomaly in the $f^3ds^2{}^5L^0_6$, $f^3dsp\ {}^7M_7$ and $f^3dsp\ {}^7L_6$ levels in UI", *Z. Phys.* D 42, 1(1997).
3. G.K. Bhowmick, R. Verma, M.K. Verma, V.A. Raman, A.R. Joshi, M.N. Deo, L.M. Gantayet, A.K. Tiwari, K.L. Ramakumar, Navin Kumar, "Preparation of electrodeless discharge lamps for emission studies of uranium isotopes at trace level" *Spectrochimica Acta 65B, 1047-1051, 2010*
4. S. Ganesan "Nuclear data requirements for accelerator driven sub-critical systems -A roadmap in the Indian context", *Pramana-Journal of Physics,* 68, 257-268 (2007).
5. Randolf Pohl, Aldo Antognini, François Nez, Fernando D. Amaro, François Biraben, João M. R. Cardoso, Daniel S. Covita, Andreas Dax, SatishDhawan, Luis M. P. Fernandes, Adolf Giesen, Thomas Graf, Theodor W. Hänsch, Paul Indelicato, Lucile Julien, Cheng-Yang Kao, Paul Knowles, Eric-Olivier Le Bigot, Yi-Wei Liu, José A. M. Lopes, LiviaLudhova, Cristina M. B. Monteiro, Françoise Mulhauser, Tobias Nebel, Paul Rabinowitz, Joaquim M. F. dos Santos, Lukas A. Schaller, KarstenSchuhmann, Catherine Schwob, David Taqqu, João F. C. A. Veloso and Franz Kottmann, "The size of the proton" *Nature* 466, 213–216 (2010).
6. R. Sánchez, W. Nörtershäuser, G. Ewald, D. Albers, J. Behr, P. Bricault, B. A. Bushaw, A. Dax, J. Dilling, M. Dombsky, G. W. F. Drake, S. Götte, R. Kirchner, H.-J. Kluge, Th. Kühl, J. Lassen, C. D. P. Levy, M. R. Pearson, E. J. Prime, V. Ryjkov, A. Wojtaszek, Z.-C. Yan, and C. Zimmermann, "Nuclear Charge Radii of $^{9,11}Li$: The Influence of Halo Neutrons" *Physical Review Letters* 96, 033002 (2006).
7. Timothy M. Roach and Dwayne Henclewoode, "Novel rubidium atomic beam with an alkali dispenser source",*J. Vac. Sci. Technol.* A 22(6), 2384 (2004).
8. Yoshihiro Iwata, Yoshizumi Inoue, Makoto Minowa, "Trace element analysis of potassium by resonance ionization mass spectrometry",Jpn. *J. Appl. Phys.* 48 (2009) 076505.

Data Acquisition and Control Electronics of Neutron Scattering Instruments under NFNBR at BARC: An Overview

R. M. Chandak, S. K. Poudel, S. S. Naik, Santosh Kumar, V. B. Kulkarni, Ismat J.A. Shaikh and R. Mukhopadhyay
Solid State Physics Division

Abstract

National Facility for Neutron Beam Research (NFNBR) has been created as a part of the Solid State Physics Division (SSPD) during early nineties to cater to the needs of the Indian scientific community in the field of neutron beam research. Scientists from BARC, other DAE units, universities and national laboratories use this facility through collaborative research projects with SSPD scientists. Many of these collaborations are being supported by UGC-DAE Consortium for Scientific Research, Board of Research in Nuclear Sciences (BRNS) and other agencies. At present the facility is mainly concentrated at DHRUVA research reactor at BARC. NFNBR has various neutron scattering experimental set-ups for basic and applied research in condensed matter. A brief description of Data Acquisition and Control Electronics associated with these instruments, developed and maintained in-house is provided.

Introduction

The short-range strong interaction of neutron with matter and its inherent magnetic moment make neutron scattering a unique probe in condensed matter research. Due to the matching of wavelength and energy of thermal neutron to the lattice spacing and excitations in condensed matter, it is an indispensible tool both for the study of structure and dynamics. Over and above, the magnetic moment of neutron makes it suitable for the study of magnetic structures and the fluctuations and excitations of spin systems. The other important advantage of neutrons over other forms of radiation in the study of structure and dynamics on a microscopic level is that they are uncharged, which allows them to penetrate the bulk of materials. They interact via strong nuclear force with the nuclei of the material and the scattering cross-section varies randomly between various elements and even between isotopes. This allows one to observe light atoms such as hydrogen in the presence of heavier ones and distinguish neighboring elements in the periodic table easily. One can exploit isotopic substitution and contrast variation methods, to gather information without ambiguity.

The National Facility for Neutron Beam Research (NFNBR) is operated by Solid State Physics Division (SSPD), Bhabha Atomic Research Centre (BARC), Mumbai. NFNBR has been built around research reactor Dhruva. The peak thermal neutron flux of Dhruva reactor is about 1.8×10^{14} neutrons/cm^2/s, when it is operated at its maximum thermal power of 100 MW.

The neutron scattering facilities are extensively used by scientists from SSPD as well as by a large number of other users. To enhance the university participation, the UGC-DAE CSR(Consortium for Scientific Research) has recently installed a neutron beam line instrument at Dhruva. At present there are about 35 active research projects from universities or national institutions using NFNBR under the UGC-DAE CSR program.

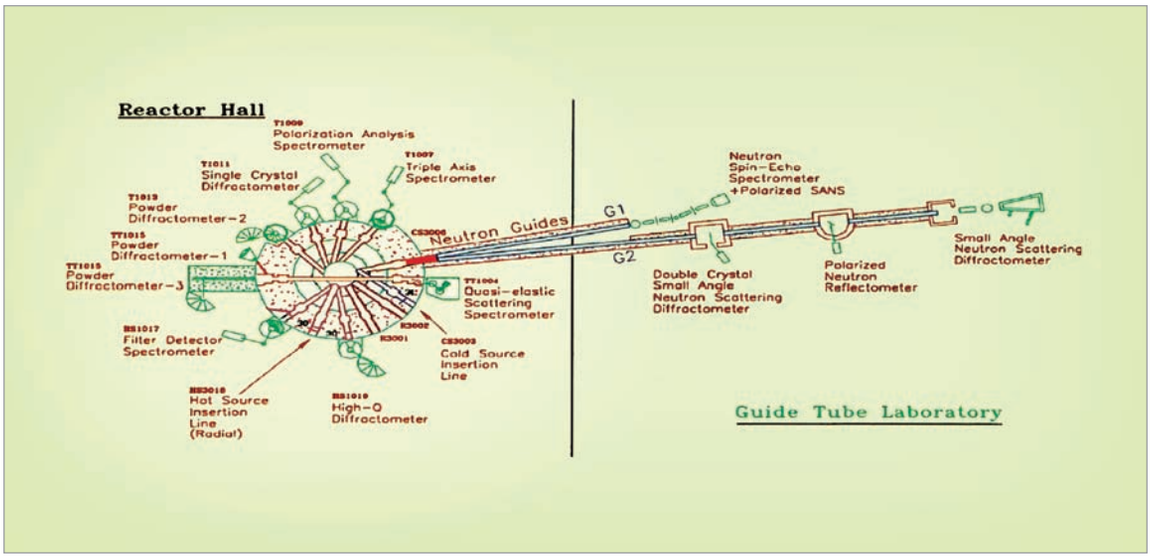

Fig. 1: Plan of the layout of the neutron scattering facility at Dhruva, BARC, Trombay.

Fig. 2: Panoramic view of the neutron instruments at Dhruva.

Plan of the layout of the beam lines at the Dhruva reactor and the neutron scattering instruments in the reactor hall and guide laboratory are shown in Fig. 1 and the photograph of the panaromic view of the neutron scattering facility at Dhruva is shown in Fig. 2.

There are twelve neutron scattering instruments under NFNBR at Dhruva reactor. Eight of them are in the reactor hall and four in the guide tube laboratory. As far as the instrumentation is concerned they fall broadly under two categories: (1) Motorized scan type and (2) Position Sensitive Detector (PSD) based. This paper gives an overview of the control and data acquisition involved in both types of instruments. The neutron scattering experiments are carried out with the sample

placed in various physical conditions by the use of sample environment systems. A brief description of these systems and their integration with the experiment control software is also given.

Motorized Scan Type Instruments

In a typical motorized scan type neutron scattering experiment, monochromatic beam of neutrons is incident on the sample being studied. Intensity of the neutrons scattered by the sample is then measured as a function of scattering angle by moving the detector in steps. Depending on the kind of instrument there could be various arms or axes to be moved to facilitate data acquisition. The schematic of one such instrument, known as Triple Axis Spectrometer (TAS) is shown in Fig. 3.

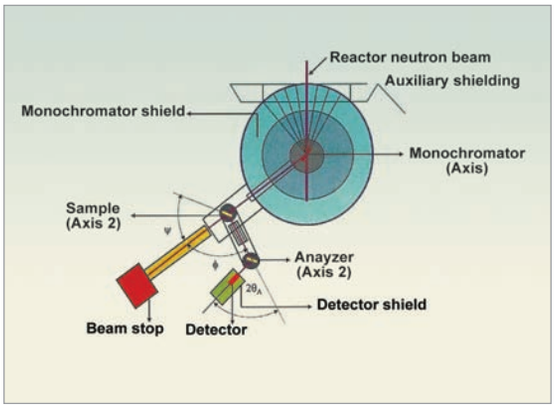

Fig. 3: Schematic of Triple Axis Spectrometer

The data acquisition consists of counting the number of neutrons scattered over an angular range, normalized either by total number of neutrons incident on the sample (monitor mode) or total time taken for the experiment (time mode). A neutron instrument has various arms/axes, like monochromator, sample, detector, analyzer, etc. The control system for these set-ups requires the precise positioning of various axes to a specified angle and acquires data from neutron detection system as a function of these angles.

The control system is designed to suit the existing mechanical and electrical assembly of the instruments. The angular movement of various arms of the spectrometer is accomplished by worm & worm-gear assembly driven by geared DC motors. The angular position feedback of the motor shaft is derived from rotary optical encoder. The principle of position control is two-speed on-off type. The motor moves in two different speeds: it begins to move fast and slows down for the last one degree. To correct backlash error while moving in reverse direction, the motor is moved one degree beyond the target position and brought back to the target in forward motion. With this scheme, in present configuration the system can control up to six motors at a time with a typical positioning accuracy of 0.01 degree.

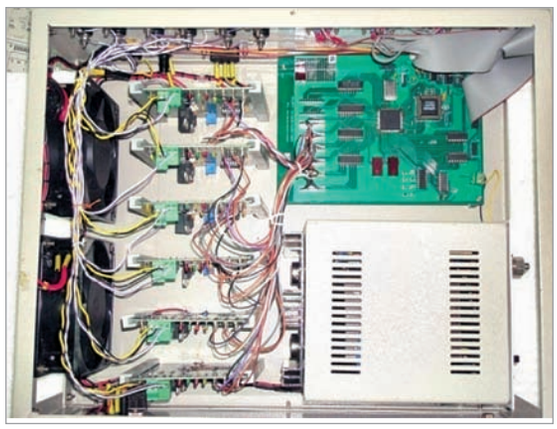

Fig. 4: Photograph of the DC motor controller card

The front end electronics for the neutron detection system typically consists of gas filled neutron detector, standard low voltage power supplies, pre-amplifier, main amplifier, discriminator-scalar and high voltage power supply. Discriminator is used to eliminate low level pulses coming from the shaping amplifier to greatly reduce contribution from pulses generated by gamma rays, in the data being recorded. Each logic pulse coming from the discriminator signifies a single neutron event detected in the detector.

The DC motor position control electronics developed at SSPD, comprises of (1) A Microcontroller and

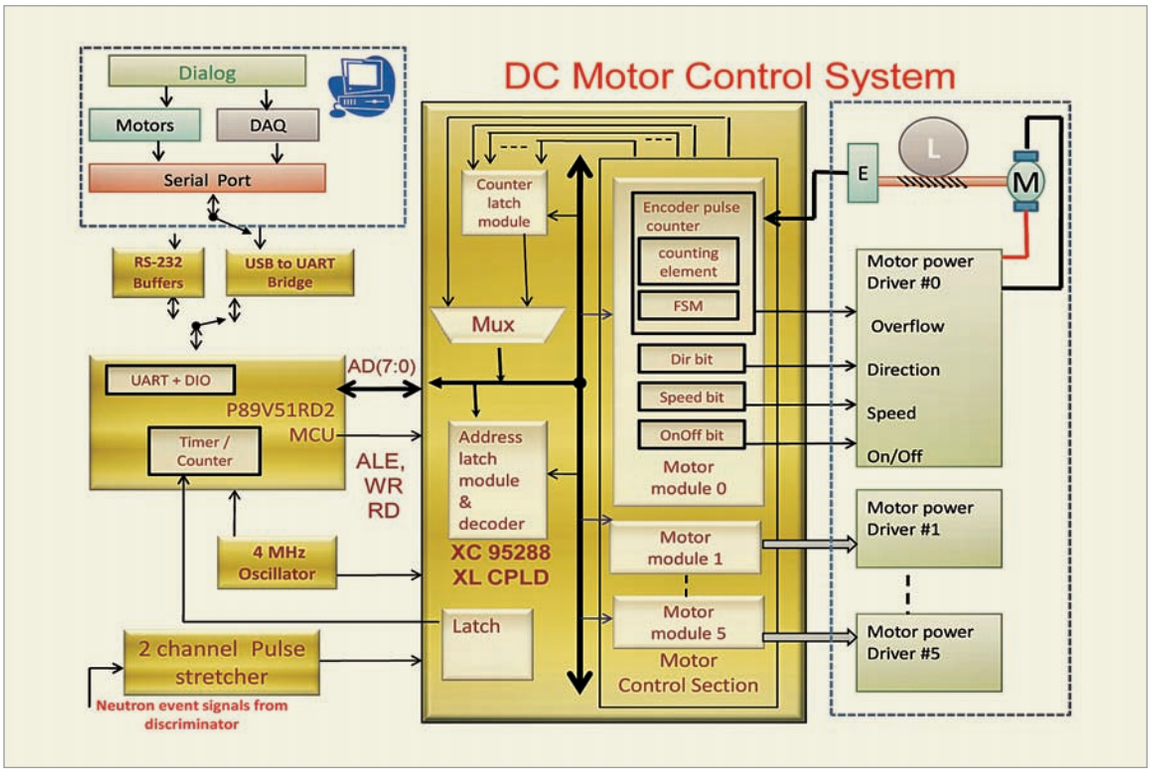

Fig. 5: Block diagram for motor control & data acquisition electronics for motorized scan type instruments.

CPLD based DC motor controller with USB interface, and (2) DC Motor Power Driver card. The internal view of the controller card and power driver card housed in the enclosure is shown in Fig. 4.

This system can control six DC motors and has two neutron-counting channels. The controller card has a CPLD for implementing control logic (with Digital outputs, encoder pulse counters, etc) of six motors. Microcontroller on the controller card exchanges data with registers in CPLD in response to command received from PC via USB-UART Bridge IC. In the motor power driver card a variable regulator is used to power an H-bridge circuit to operate the motor in a desired direction at slow/fast speed. The various control inputs to the motor power driver card and the architecture of the entire system is as shown in Fig. 5.

For the PC application programs suitable motor control and data acquisition routines are also developed. The software has five operating modes: (1) Manual Mode, (2) Rocking Mode, (3) Energy Scan Mode, (4) Look-Up File Mode and (5) Continuous Time Scanning Mode.

Position Sensitive Detector (PSD) based neutron scattering instruments

The Position Sensitive Detector (PSD) is widely used to measure the position co-ordinates of neutrons. A typical, linear 1D neutron PSD is a cylindrical He-3 gas filled detector of one inch diameter and length of one meter. It has a high resistive anode wire of 25μm diameter of specific resistivity 10k&!/m. The gas is usually kept at a pressure of 8 to 10 bar. The detector works in the proportional counter region.

In a PSD type neutron scattering experimental set-up, intensity of the neutrons scattered by the sample is measured by using PSD(s), without having to move the detector. The basic electronics set-up for position encoding electronics is shown in Fig. 6.

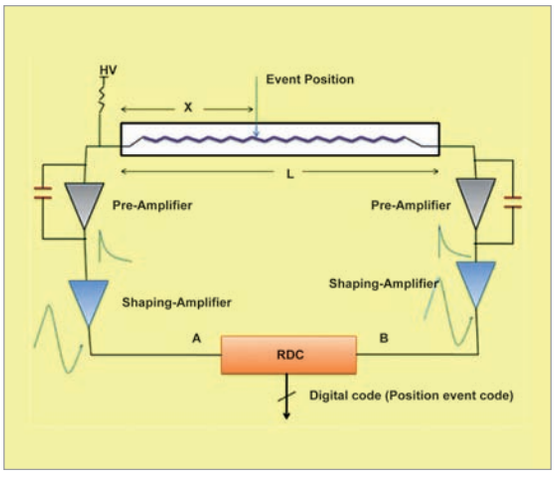

Fig. 6: Position encoding electronics of a PSD.

The nuclear electronics system for each PSD essentially comprises of two pre-amplifiers, two shaping amplifiers, and a Ratio ADC (RDC). These modules are designed by Electronics Division, BARC and now manufactured by ECIL. During the course of experiment, RDCs provide the event code, which signify the position where neutron was detected. These nuclear electronic modules give the position of neutron event by the principle of Charge Division Method. In a typical system at Dhruva reactor, up to five one-meter long PSD are used to cover the angular range of interest as shown in Fig. 7.

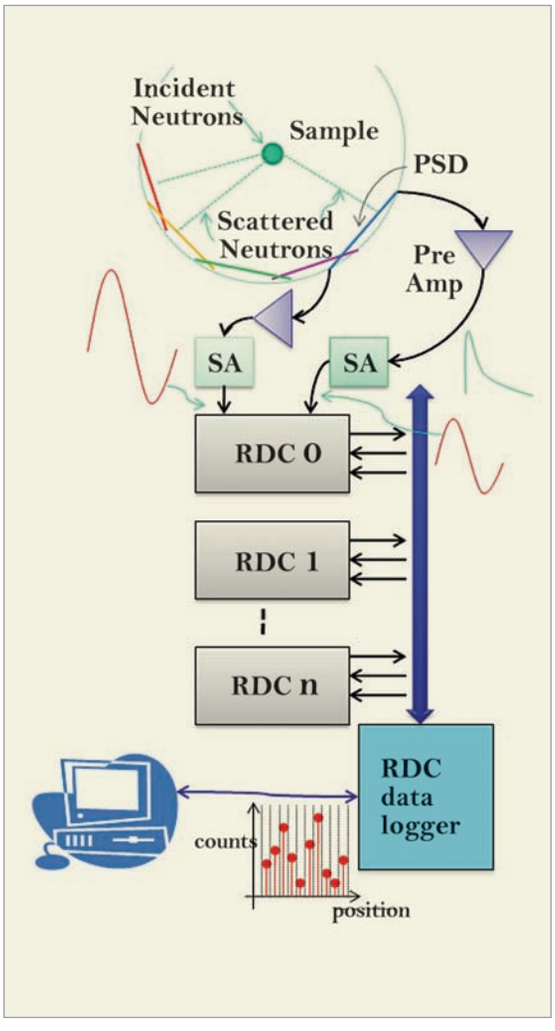

Fig. 7: PSD type neutron scattering experimental

The total ionisation charge Q produced in the avalanche at a distance X from one end of the detector divides itself and flows to the two ends of the detector. Depending on the position of detection of neutron the amplitude of the two signals differ from each other. Based on charge division principle it can be shown that $\frac{V_b}{V_a+V_b}=\frac{X}{L}$ for small Z where Z is the input impedance of the charge sensitive pre-amplifier. The charge sensitive pre-amplifier integrates the charge that is collected at both the ends of the detector and produces a voltage pulse at the output. The pre-amplifier should have low input impedance so that the position of the neutron event and the amplitude of the detector pulses vary linearly. The shaping amplifier takes the exponential tail pulses from the pre-amplifier and shapes it into quasi-Gaussian pulses. The output of the pre-amplifier have sharp peaks, so shaping of the pulses has to be done in order to get sufficiently flat peaks

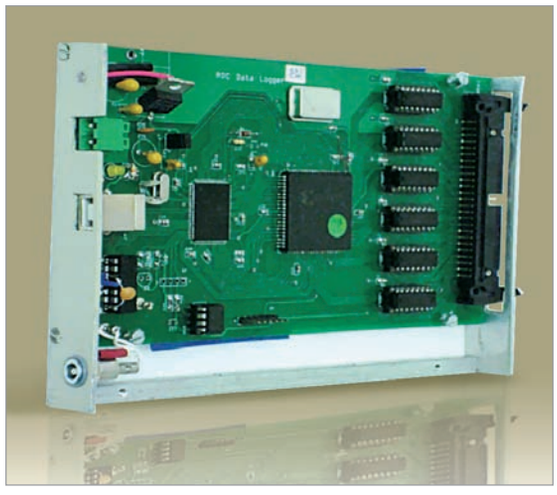

Fig. 8: The Data logger card

so that the peak amplitude could be sampled for position encoding. The outputs of the two shaping amplifiers from the two ends of the detector (V_a and V_b) are fed to Ratio to Digital Convertor (RDC) which finally gives digital code proportional to $\frac{V_b}{V_a+V_b}$, specifying the position of the neutron event.

A High Speed USB based RDC Data Logger card which is shown in figure 8, has been made at SSPD, BARC, for logging data from multiple RDCs to PC. A CPLD on the card continuously polls the RDCs for data, and fills it in the FIFO memory of a high speed USB microcontroller. Readout of RDCs is made over a 24 bit RS-422 multi drop parallel bus connecting all RDCs to the Data Logger, which generates the bus cycle timing diagram to read a RDC. The 24 bits on bus consists of 16 data or status bits, 4 address bits and 4 handshake bits. The data and status bus are multiplexed.

A VC++ based program developed for these neutron scattering experiments reads event codes from FIFO of microcontroller and builds spectrum on PC. This program sweeps physical parameters of sample and collects PSD data for pre-determined

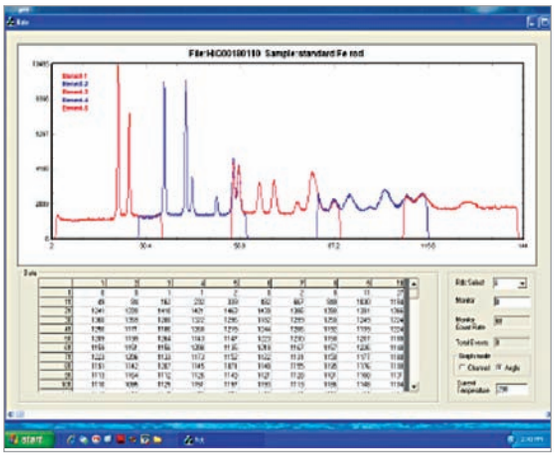

Fig. 9: On-line display of data recording

monitor counts. Figure 9 shows diffraction pattern seen on the user interface screen of this program.

The Data Logger cards installed on six instruments under NFNBR at Dhruva are working satisfactorily. The event rates at which the RDCs give data do not see any communication bottlenecks. By filling FIFO by test data we found the peak rate at which data could be logged is 150000 bytes per second.

Sample Environment Set-ups and their control equipment:

Various Sample Environment Set-ups existing at NFNBR enable the study of neutron scattering from materials under various physical conditions such as temperature, pressure, magnetic field, etc. The data acquisition software described above is integrated with various sample environment control equipments. The computer interface to these instruments is done on RS-232, RS-485, GPIB, etc.

The various sample environment set-ups include (1) CCR or cryostat based Low temperature set-ups for varying sample temperature over 1.5 K to room temperature, (2) A high temperature neutron scattering furnace, (3) Flipper coils for control of polarization of incident neutron beam on sample and (4) a cryogenic magnet for collecting neutron diffraction data from a sample in presence of magnetic field up to 7 Tesla.

Summary

An overview is provided of the data acquisition and instrumentation control, developed in house, for the instruments available under national facility for neutron beam research at BARC. It is found that this in-house development has helped immensely as maintenance is much easier and faster. This has resulted in better availability of the instruments to the researchers.

Acknowledgements

We would like to thank Dr. S.L Chaplot Head, SSPD for his constant encouragement and support. We are thankful to Dr. S.M. Yusuf, SSPD for his keen interest and valuable suggestion in the course of writing this article.

References

1. S. K. Poudel, V. B. Kulkarni, Santosh Kumar, R. M. Chandak, P.S.R. Krishna, R Mukhopadhyay, High Speed USB Data Logger for Position Sensitive Detector Data Acquisition, National Symposium on Nuclear Instrumentation, Mumbai. February-2010.

2. R. M. Chandak, V. B. Kulkarni, Santosh Kumar, S. S. Naik, I. A. Shaikh, R Mukhopadhyay, S. K. Poudel, Stepper Motor Control System for Neutron Focusing Devices, at Conference on Neutron Scattering and Mesoscopic Systems, Goa. October 12-14, 2009. pp 135.

3. S. S. Naik, Ismat Kotwal, R. M. Chandak, V.G.Gaonkar, Data Acquisition & Instrument control system for neutron spectrometers, Pramana-Journal of Physics, Vol. 63, No.2, August 2004, pp. 455-458.

4. D Sen, V. K. Aswal, R. Mukhopadhyay and S. L. Chaplot, National Facility for Neutron Beam Research, Published by SIRD, BARC.

5. Utilization of Research Reactor, (Eds. S. M. Yusuf and A. V. R. Reddy) IANCAS Bulletin I(3) 2002.

BARC Medical Cyclotron Facility: Performance and Achievements in the First Decade after Commissioning

M.G.R. Rajan, Saikat Nandy, N. Lakshminarayanan, B.K. Sharma, Arpit Mitra, Amit Kumar,
Shrinibas Nayak, Kanchan Kushwaha, Arjun G, R. Chinagandham, Yuvraj N.

The installation and commissioning of the BARC Medical Cyclotron Facility (MCF), in October 2002, was a landmark event for very important reasons. It was the first cyclotron in the country for producing short-lived positron emitting isotopes for positron emission tomography (PET) - a nuclear medicine investigation procedure - with proven use in oncology, cardiology and neurology. The nuclear medicine fraternity in the country was eagerly awaiting to use this modality for the benefit of cancer patients in the country; and within a short time it removed the apprehensions of the nuclear medicine centres about the economic viability of investing in such high cost equipment. The decision by the Department of Atomic Energy and the BARC, to set up the facility at RMC, was taken after much deliberation and fact finding. Details of this and of the installation of the MCF in the Tata Memorial Annexe Building, Parel, where RMC is situated, which involved the will and determination of a team of DAE scientists and engineers is beyond the scope of this article and is detailed elsewhere (see footnote[1]).

The MCF and the PET scanner were installed at the same time and were dedicated to the nation on October 31, 2002 by the then Prime Minister of India. The MCF is in an area of less than 135 M^2 and has an unshielded PETtrace cyclotron from General Electric (through Wipro-GE,India), two FDG mini modules, one carbon-11 methylation module, a dispenser to aseptically distribute the ^{18}F-FDG into vials for distribution to hospitals, a module to make ^{15}O-water installed in the PET-scanner room in the first floor, where the $^{15}O_2$ is directly sent from the cyclotron due to its $T_{1/2}$ of 2 min. All the hot cells and the synthesis modules were from M/s Nuclear Interface, Germany, who is a pioneer in this field (now taken over by GE-Healthcare).

With some training from the application specialists from GE for the medical cyclotron and the PET-radiochemistry synthesis modules, several trial batches of ^{18}F-FDG were successfully made. Following this, ten production batches and their QC (quality control) testing was carried out as per the US-Pharmacopoeia specifications including animal bio-distribution, and the data compiled and submitted to the Radiopharmaceuticals Committee (RPC) for clearance. The RPC is an oversight committee appointed by the Department of Atomic Energy to oversee and approve the production and QC processes of radiopharmaceuticals (RPs) in DAE units, for their use in humans. The RPC approved ^{18}F-FDG as a radiopharmaceutical product on October 28, 2002, and the next day a lot of ^{18}F-FDG was made and administered to the first human volunteer, Dr. Ramamoorthy, and the first FDG-scan was performed in India.

Regular production soon commenced, but there were initial teething troubles, and regular, uninterrupted routine production and supply to hospitals started from March 2003. To begin with, RMC was the only consumer of the MCF. The Hinduja Hospital started procuring 18F-FDG soon after and the consumer base of MCF expanded gradually

[1] Booklet brought out on the occasion of the BRNS – Theme meeting, 'A Decade of Operation of the BARC Medical Cyclotron Facility' held on October 18, 2012.

Fig. 1A: BARC Medical Cyclotron Facility in the basement of TMH Annexe Building

Fig. 1B: PETtrace 16.5Mev cyclotron in vault in the MCF

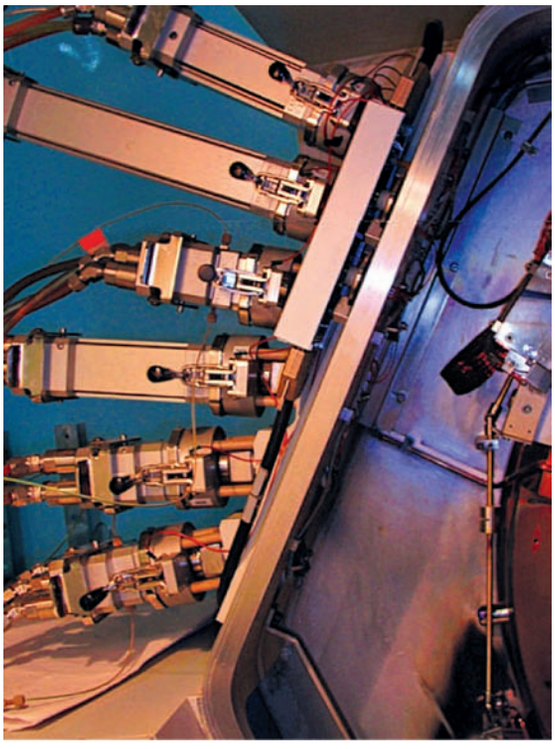

Fig. 1C: Liquid and gas targets in the cyclotron

Fig. 1D: PET-Radiochemistry synthesis and dispensing modules

Fig. 1E. PET-Radiochemistry room – ready for the day's activities.

as other nuclear medicine centres procured PET-CT scanners. Table 1 shows the expanding consumer base for ^{18}F-FDG over the years. Most of them are regular customers of the MCF but a few are now procuring ^{18}F-FDG from another medical cyclotron facility in the private sector. By this, we have ably proven that the central MCF with several satellite PET-CT scanners is possible and commercially viable in India too. Table 2 shows the ^{18}F-FDG sales over the years since 2003.

Table 1: Expanding customer base for ^{18}F-FDG produced at the MCF

Year	Nuclear Medicine Centres using [F-18]FDG from the MCF
2002	Radiation Medicine Centre
2003	P.D. Hinduja Hospital, Mahim, Mumbai
2004	Jaslok Hospital & Research Centre, Peddar Road, Mumbai Bombay Hospital, Marine Lines, Mumbai Tata Memorial Hospital, Parel
2007	Mandakini Nuclear Imaging & Research Centre, Chembur
2008	SPECT-Lab, PuneSRL-Diagnostic, Worli, MumbaiShreeji Imaging & Diagnostic Centre, Borivalli, Mumbai RUBY Hall Clinic, Pune
2009	KEM Hospital, Parel, Mumbai
2010	Nanavati Hospital, Vile Parle, Mumbai ACTREC, Kharghar, Navi Mumbai
2011	Seven Hills Hospital, Andheri, Mumbai

The sale of ^{18}F-FDG (and other ^{18}F-RPs) from the BARC MCF is permitted following a policy decision that the Medical Cyclotron Facility will be operated jointly by staff from RMC, BARC, and BRIT. The revenue generated from the sale of PET Radiopharmaceuticals is credited to BRIT. The overall the facility is supervised by the Committee for the Management of Medical Cyclotron (CMMC), constituted by Director, BARC and Chaired by Chief Executive, BRIT.

There is a perception amongst nuclear medicine physicians, largely due to the information from sales persons from cyclotron vendors, that the production

Table 2: ^{18}F-FDG Sales over the years since 2003.

Financial Year	Rupees (in Crores)
2004-05	2.02
2005-06	4.27
2006-07	4.68
2007-08	5.43
2008-09	4.67
2009-10	4.89
2010-11	5.8
2011-12#	5.6

#Sales in 2011-12 did not meet the target of Rs. 6 Cr due to several days of shutdown due to equipment failures.
This does not include the sales of [F-18]NaF, [F-18]FLT and [F-18]FMISO. The total sales of these three are small and was Rs. 5.92 lakhs in 2011-12.

Table 3: Production Data (as of Sept 2012)

Radiopharmaceuticals	No. of Batches
[F-18]FDG	3715
[F-18]NaF (commenced form 2007)	535
[F-18]FLT (commenced from 2010)	95
[F-18]FMISO (commenced from 2010)	61

The pricing ^{18}F-FDG was based on a costing-model and customers were charged for the activity supplied at the time of delivery, rather than per patient dose. Customers were requested to come to the MCF and take delivery and transport it to their site on their responsibility. This pricing model has been appreciated by the customers who, on the whole, find the prices from the MCF to be the lowest, since we do two production runs in a day and, hence, costs due to radioactive decay are kept to a minimum.

From March 2003 to 2006 there were no problems with the cyclotron and auxiliary equipment, except for occasional synthesis failures due to operator errors or failure in the solenoid valves or tubings. The latter was identified as due to radiation damage and this was sorted out by introducing a flush program after synthesis, where clean water was made to pass through the tubing and valves to wash away any residual radioactivity, and this made a big difference to the reliability of the valves, tubings and reduced replacement costs. We could reduce the costs of spares very significantly, by sourcing them directly from the manufacturers rather than from GE.

The uptime from March 2003 to March 2006 was 99% except for the planned shutdown for preventive maintenance, lasting 2 weeks every six months. This long period disrupted the FDG diagnostic studies at all nuclear medicine centres dependent on us. Shut down maintenance was a necessity and after much planning and discussion with Wipro-GE, this was brought down to one week every six months and the last Monday of every month. When necessary, our staff along with the health physicists worked on weekends and late nights to ensure there was minimum disruption in supply of ^{18}F-FDG.

As nuclear medicine centres, other than RMC, started installing PET-scanners, the need for making more FDG became necessary and we started making two batches a day and we could cope with this as there were two FDG synthesis modules available. The high yield fluorine-18 liquid target (mentioned above) installed at this time (in the X-Plan) also helped. Our health physicists did a detailed survey of the air activity during production and the air activity released from the stack before giving us this clearance. A major limitation due to the compact area of the facility, in producing more than 130 GBq (3.5 Ci) of fluorine-18 in the cyclotron, was that the radiation in the area outside the cyclotron vault door would exceed the threshold of 0.1 mR/h and the area gamma monitor would sound an alarm and trip the cyclotron, although the chemistry modules are designed to handle 185GBq (5Ci).

Timely production also required staff to reach the MCF unfailingly and the sense of unstinted responsibility of the physicists and chemists made this possible. Everyone at the MCF felt the need to make every synthesis work. Disruption in ^{18}F-FDG supply meant i) making the fasting patients' wait (ii) make the nuclear medicine physician unhappy (iii) loss of revenue to BRIT and importantly (iv) a loss of reputation for an institute of BARC's strature. In addition, a failed synthesis also meant a loss of expensive ^{18}O-water, FDG-precursor and other chemicals and man-rem expenditure. Timely availability of FDG was put to test when a demand was made by a customer in early 2009 to supply the ^{18}F-FDG at 8 AM. This required that the staff come in at 6 AM and start their work. The MCF staff and heath physicists unanimously agreed to do so and it is a source of great pride to the MCF team that it has remained competitive in the market.

The first major problem in the cyclotron suddenly occurred one day in early 2006, when the copper helium heat exchanger developed a leak inside it and the cyclotron tripped. It was a specially designed heat exchanger and not available locally. We had to wait for a full week before it was located at one of the GE's many PETtrace units worldwide and shipped to Mumbai. This was instrumental in introducing a shut-down maintenance on the Monday of every month to identify potential vulnerabilities and rectify them.

Wipro-GE was also on the learning curve with us in terms of cyclotron operations and maintenance. In fact, our MCF was a showcase for them to sell more of their machines in India. This somewhat improved the availability of spares as there were more installations. It is noteworthy that all engineers appointed by Wipro-GE for cyclotron and PET chemistry have had a stint at the MCF before they were posted elsewhere.

By 2006, we had achieved a fair level of competence in the production and supply of ^{18}F-FDG and an urge to make other ^{18}F-radiopharmaceuticals (RPs), and not just be a run-of-the-mill ^{18}F-FDG supplier, was felt. This was the PET era and there were publications that were appearing regularly on the production and use of other ^{18}F-RPs. We required a shielded synthesis module for doing this as well as for doing a third FDG run if necessary. The C-11 methylation module was hardly used due to two reasons; first, the synthesis module was designed to trap the $^{11}CO_2$ from the cyclotron and convert it to $^{11}CH_3I$ and use it for labeling. Several batches of ^{11}C-methionine were made but with low yields, even at the hands of the application specialist who visited here for this purpose - a known limitation of ^{11}C-RPs made by this route. Secondly, there were little commercial prospects for ^{11}C-RPs due to its 20 min $T_{1/2}$ since the entire cyclotron run and synthesis was adequate for only one patient study, making it prohibitively expensive, in comparison the same effort and cost in making ^{18}F-FDG would benefit several cancer patients. We modified the C-11 module by rerouting the tubing and changing the human-machine-interface (HMI) and rewriting the program in the built-in NINA® software for nucleophilic fluorination and it was a day of great satisfaction that we could make ^{18}F-FDG with it. Hence, a standby synthesis module was made available for doing the third ^{18}F-FDG synthesis, if required, and also for doing R&D to synthesize other ^{18}F-RPs.

The first ^{18}F-RP we made was ^{18}F-NaF, a simple molecule produced in the cyclotron target when ^{18}O-water is irradiated. To make it suitable for patients' use, it was necessary to make it free from radioactivity that came from the target and Havar foils. We did this by trapping the $^{18}F^-$ in an anion exchange column and eluting it. Several trials and testing were done and the data submitted to the RPC for approval, which came in 2006. We started regular production and regular deliveries to our customers soon after that.

Next, we took up the challenge of making ^{18}F-FLT and ^{18}F-FMISO that are important for analysis of tumour proliferation and hypoxia, respectively. We also chose to use solid-phase extraction methods for purification as this would simplify the production and avoid the additional time required for the semi-preparative HPLC purification, which is quite a cumbersome process. This involved a fair degree of R&D activity and simple solutions were obtained for both. After much trials and product evaluation, we could get the RPC approvals for the production and QC monographs in 2010. Regular production and supply is presently being made on a weekly basis.

We have also standardized the methods to make ^{18}F-FAZA and ^{18}F-FES and are in the process of obtaining RPC's approval for them. There are efforts to make ^{18}F-FET, for imaging brain tumours, ^{18}F-Choline and ^{18}F-fluoroethylacetate for prostate imaging.

What we sorely require is an electrophilic synthesis module and an $^{18}O_2$ gas target for making $^{18}F_2$ to produce ^{18}F-FDOPA, with reasonably high specific activities, to meet the requirements from many nuclear medicine centres. We also need a full-fledged nucleophilic fluorination module with a semi-preparative HPLC and a tongs-manipulator. However, these appear to be wishful thinking as presently there is space for just one module that too with a load restriction of 5 tonnes (instead of a 9 tonne actual requirement).

Severe constraints were experienced on two occasions due to the non-availability of ^{18}O-water

Fig. 2A and B: The cyclotron run is on and radio-activity will be delivered to hot cell(s) at ~6:15 AM & ~11:00 AM

^{18}O-water is produced only by a few manufacturers worldwide. Fortunately, the lead author's training at Dr. Nebeling's lab at Hamburg helped. The technology learnt there was employed to distill the recovered ^{18}O-water (to remove the solvent impurities and the long-lived activity leaching from the target and Havar foils) and the recovered ^{18}O-water made reusable. Although the target had to be irradiated for a longer period due to a decreased ^{18}O-content in the recovered water, the production and supply of ^{18}F-FDG continued uninterrupted.

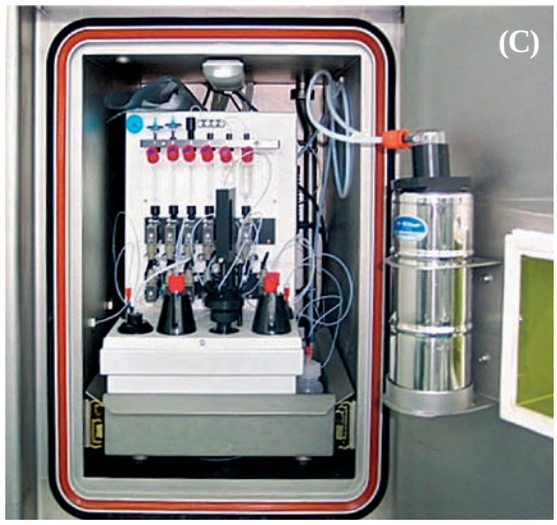

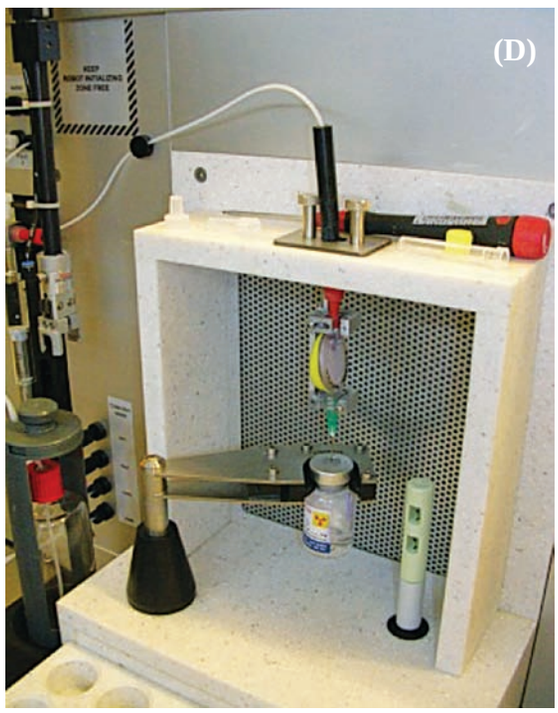

Fig. 2C,D &E: ~7:45 AM & ~12:30 PM The chemists overseeing the production, aseptic dispensing and QC of [F-18]FDG

Fig. 2F: Health Physicist monitoring the [F-18]FDG consignments ~8:00 AM & ~ 12:00 noon

Two additions that helped the overall GMP are the installation of an air-shower at the entrance to the Radiochemistry area and a 20 minute kinetic LAL test so that the ^{18}F-FDG product is released with this assurance.

In the cyclotron front, we have upgraded the radioactive waste-gas compression system, installed a large capacity oil-free dry air compressor, a radioactivity monitor at the stack for a real time assessment of activity released. This showed that the radioactivity released from the MCF is much below permissible levels.

Niobium metal, because of its chemical inertness compared to silver and other metals, is now the preferred metal for making target cavities. The advantage is that there are fewer requirements for target maintenance. However, it is costly and we have indigenously fabricated and tested a low volume niobium target cavity for use in the Target No. 2 position. The results are very encouraging and we will do this for Target No. 4.

We are in process of developing our own PLC-based synthesis module for ^{18}F-FDG. To begin with, we have developed a simple PLC-based and a manual module for making ^{18}F-NaF, which is required daily by TMH and others. This will make the fluorination module available for more R&D work.

With the MCF running successfully over the years, with an uptime close 95%, and the importance of ^{18}F-FDG in cancer diagnosis and management well established, there is confidence in the hospital management in India that medical cyclotron facilities are financially viable in India. As a result, over 15 cyclotrons have been installed in the private and public sectors in the country. However, their requirement for qualified staff has led to some attrition of physicists and chemists from our MCF.

Cyclotrons are sturdy machines and are expected to last for decades. Ours has served us well for a decade. While the basic design of the magnet, RF system, ion source, vacuum, and beam extraction has not changed, what have changed are the electronics, fluidics and software, which were designed two decades back (in 1992). What we now have is reaching obsolescence and spares are not readily available with the service providers. We need a major upgrade of these to keep producing ^{18}F-FDG routinely and meet the growing demands. Space for new synthesis modules will be required for R&D and to make other ^{18}F-RPs as per requests.

Our need to find space to put up more synthesis modules led us to approach Dr. R. Badwe, Director, TMC to give us space adjoining the MCF. We were pleasantly surprised by his suggestion that we put up a full-fledged medical cyclotron facility at ACTREC in the building planned as a joint Radiation Research Unit for BARC and ACTREC. This proposal will be a part of the XII-Plan and the facility will be built around an 18–20 MeV cyclotron with electrophilic and nucleophilic fluorination modules, C-11 methylation modules and modules to make I-124 and Cu-64 labeled radiopharmaceuticals. This will be an important initiative for sustaining the momentum on PET-based diagnosis.

(The R&D work done at the MCF has resulted in 7 publications, 9 conference abstracts and chapters in three IAEA publications.)

Electrochemical Techniques For Nanoscale Surface Engineering (ECTNSE-2012)

Scientific Programme of the event

Electrochemical techniques, well established in the area of surface engineering, are now being deployed to modify surfaces at the monolayer and nanometer scale to generate exciting developments in the fields of spintronics, biomedical implants, solar energy and metallurgy. The objective of this meet was to provide a forum for scientists and engineers to discuss the role of Electrochemical Techniques in the developing field of Nano-Technology and the emerging trends in these areas. The topics covered included (a) GMR based Multilayers for Sensors; (b) Electrodeposited materials for Energy Research; (b) Surface modification for Biomedical implants; (c) Nanocomposite coatings for industrial Applications; (d) Characterization of modified surfaces; (d) Electrodeposition from non-aqueous electrolytes (covering Nuclear applications). The scientific program of the meeting consisted of fourteen invited talks by eminent scientists / engineers from national and international institutes and contributed papers in oral/poster sessions.

Highlights of the event

Eighty delegates, including three from abroad and ten students, attended the workshop. Dr. A. K. Suri, Director, Materials Group, Bhabha Atomic Research Centre inaugurated the workshop highlighting the importance of Surface Engineering in extending the life of structural materials including nuclear materials, for different sensor applications and for bio-medical implants. There were 14 invited talks, 5 contributed oral presentations and 15 poster presentations. Prof. Sudipta Roy, Newcastle University, UK emphasized the importance of electrodeposition from ionic liquids on surface engineering and Dr. Imre Bakonyi described in detail towards sensor fabrication using electrodeposited nanolayered multilayers. Dr. Kamachi Mudali, IGCAR highlighted usefulness of surface engineering especially in nanoscale on corrosion resistance of materials. He also pointed out organization of such workshop in frequent manners to educate younger scientists and engineers so that electrochemical materials science research turns into societal benefit.

Inauguration of the workshop by Dr. S. Kailas, Director, Physics Group, BARC

BRNS Theme Meeting: A Decade of Operation of the BARC Medical Cyclotron

A one- day BRNS Theme Meeting was held on 18th October 2012 to commemorate the 10 years of successful operation of the first Medical Cyclotron Facility (MCF) in the country located at the Radiation Medicine Centre (RMC), Parel. Dr. Ratan Kumar Sinha, Chairman, Atomic Energy Commission and Secretary, Department of Atomic Energy delivered the inaugural address. A booklet highlighting the history of the MCF, its performance and articles from its users was released by Dr. Sinha. Dr. Sinha complimented the men behind the MCF operations for the excellent performance and services rendered. The staff members of the MCF drawn from BARC and BRIT had also been rewarded earlier with the DAE Group Award for their achievements.

Dr. K.B. Sainis, Director, Bio-Medical Group, in his opening remarks complimented the MCF Team for running the facility with a high uptime and supplying [F-18] FDG to several hospitals in Mumbai and Pune. Dr. A.K. Kohli, Chief Executive, BRIT, said that the systematic efforts and commitment of all the MCF staff, including those who have superannuated, or left for better prospects, has made the MCF work reliably and keep the customers satisfied.

The Theme Meeting received reminiscent account from former colleagues, who played a key role in executing the IX-Plan Project of setting up the MCF, apart from learning from the users about patient services rendered possible with FDG and other F-18 radiopharmaceuticals supplied from the MCF. The impact PET imaging has had in managing patients (oncology and non-oncology) was highly emphasized. There were three Sessions of invited talks, covering (i) the project phase experience and the overall progress in the field, (ii) clinical services and valuable support in management of patients of cancer and other diseases/disorders and (iii) progress made in PET-CT imaging systems and detectors and importance of PET-tracers beyond FDG. M/s GE-Healthcare India, the supplier of MC to BARC, shared their valuable learning experience in working with the MCF team in maintaining the equipment and the future upgrades that are possible to keep the cyclotron and its accessories running satisfactorily.

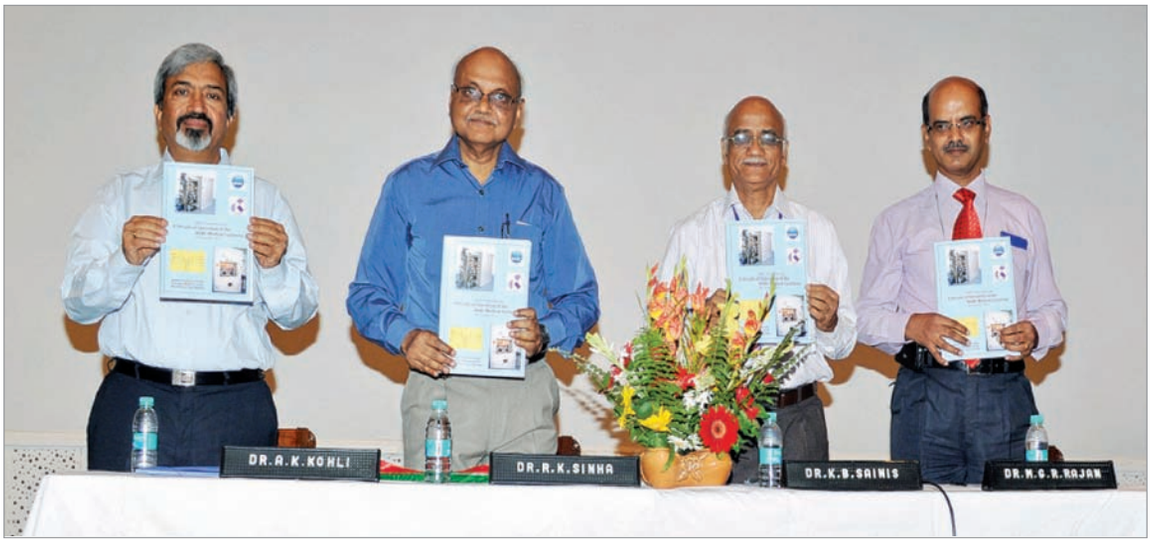

Dr. R.K. Sinha, (second from left) Chairman, AEC, releasing the booklet on the occasion

Report on "Training in Personnel Monitoring Procedures (TPMP-2012)"

A four-day workshop on "Training in Personnel Monitoring Procedures (TPMP-2012)" was conducted by the Radiological Physics and Advisory Division, BARC during October 9-12, 2012 at HP auditorium, CTCRS Building, Anushaktinagar. The workshop was supported by the Board of Research in Nuclear Sciences. The aim of the workshop was to provide training to the employees involved in personnel monitoring related activities at various TLD laboratories located in different parts of the country.

Dr. Y. S. Mayya, Head, RPAD, welcomed the participants. The Chief Guest, Shri S. Duraisamy, Vice-Chairman, AERB in his inaugural address stressed on the need for a systemized procedure in personnel monitoring. He also informed that AERB has taken up the issue of registering all the X-ray facilities in the country which would expand the personnel monitoring activity. In his presidential address, Shri. G. Nageshwara Rao, Director-Operations, NPCIL, spoke on the strictness of radiation protection practices being followed at NPCIL plants to keep the personnel exposures to as low as achievable levels. Dr. B. K. Sapra, Head, Environmental and Biodosimetry Section, RPAD proposed the vote of thanks. The function was attended by several officers from BARC, AERB and NPCIL.

The formal announcement regarding accreditation of the seven NPCIL TLD laboratories, subsequent to the signing of Memorandum of Understanding between BARC and NPCIL was made during the Inaugural function. The accreditation certificates were distributed to the representatives of the seven NPCIL TLD laboratories located at various NPP sites by Shri S. Duraisamy.

A total of 45 delegates nominated by 16 TLD Units of BARC/NPCIL, accredited laboratories from private sector/defence and AERB attended the workshop. The technical programme consisted of 18 lectures delivered on various topics pertaining to Personnel Monitoring. Three practical cum hands-on training sessions of 3 h duration each were also conducted for the participants.

(L-R): Sh. Nageshwara Rao, Dr. B.K. Sapra, Shri S. Duraisamy and Dr. Y.S. Mayya at the inaugural function of TPMP-2012

Report on BRNS-Young Scientist Research Awardees' Meet (YSRAM)

The Basic Sciences Committee (BSC), BRNS organized a Young Scientist Research Awardees' Meet (YSRAM) in a symposium mode, during November 26-28, 2012 at the Multipurpose Hall, BARC Guest House and Training School Hostel, Anushaktinagar, Mumbai. In this Meet, 42 active Principle Investigators (PI) of the ongoing YSRA projects and 2 PIs who had recently completed their projects, presented the progress made in their projects. Besides these PIs, 40 young scientists from BARC, 23 new project proposers and 40 young academics from various parts of India were delegates to YSRAM. The technical content of the two day YSRAM consisted of presentations by PIs of the ongoing projects and special lectures by experts. The new YSRA applicants presented their proposals before experts on 28th November, 2012.

The inaugural function was presided over by Dr. S. Kailas, Director Physics Group, BARC and Chairman, BSC, BRNS. Dr. A.V.R. Reddy, Member Secretary, BSC welcomed all the participants, experts, members of BRNS and invitees to YSRAM. Dr. Kailas in his presidential address spoke about BRNS activities pertaining to basic sciences and collaborative projects for collective growth. Dr. S.G. Markandeya, Controller, BARC and Scientific Secretary, BRNS in his keynote address spoke on Atomic Energy programme in India and the opportunities in the Department of Atomic Energy. He also gave an overview on the Past, Present and future collaborative R&D activities initiated by BRNS. Dr. Sangeeta, Programme Officer, BRNS, Dr. N.K. Sahoo, Secretary, Physics, BRNS and Dr. J.R. Bandekar, Secretary, Biology, BRNS shared their views and impressions about BRNS-YSRA scheme. Dr. Kailas released the pre-proceeding volume and Dr. Markandeya released the CDs containing the pre-proceeding volume and PDF files of all the publications of the ongoing YSRA projects.

Shri Sekhar Basu, Director, BARC, addressing the gathering during the valedictory function of YSRAM

"....YSRAM is a forum that provided an opportunity to young delegates in the same age group, with similar aspirations, to interact with each other...."

Index

January-February 2012

Articles

Brief Communications

March-April 2012

Articles

- **Design and Application of a Formal Verification Tool for VHDL Designs**
  Ajith K. John, A.K. Bhattacharjee, Mukesh Sharma, G. Ganesh, S.D. Dhodapkar, B.B. Biswas
  Reactor Control Division
- **Development and Fabrication of LEU Plate Fuel for Modified Core of APSARA Reactor**
  G. J. Prasad, V. P. Sinha, P.V. Hegde
  Metallic Fuels Division
- **Development of Carbon / Carbon Composites for Nuclear Reactor Applications**
  Ramani Venugopala, D. Sathiyamoorthy, A K. Tyagi
  Powder Metallurgy Division & Chemistry Division
- **Frontiers in Science of Cutting Edge Technologies: Physics Group in BARC**
  S. Kailas
  Physics Group
- **Photocatalytic Hydrogen Generation from Water using Solar Radiation**
  R. Sasikala and S. R. Bharadwaj
  Chemistry Division
- **Searching for the Proverbial Needle in a Haystack: the Information Dilemma**
  Sangeeta Deokattey and K. Bhanumurthy
  Scientific Information Resource Division
- **Zinc Oxide Nanowires for Gas Sensing Application**
  Niranjan Ramgir, Niyanta Datta, Manmeet Kaur, S. Kailasaganapathi, A.K. Debnath, D K. Aswal and S.K. Gupta
  Technical Physics Division

Brief Communications

- **Controlled Uptake and Release of Phototherapeutic Porphyrin Dye using Surface Functionalized Silver Nanoparticle Conjugates**
  Chemistry Group
- **Designing Novel Nanomaterials for Application in Nuclear Waste Management**
  Chemistry Group
- **Development of Peptide Mimic Shell Cross-linked Magnetic Nanocarriers for Theragnostic Applications**
  Chemistry Group
- **Hot Vacuum Extraction- Quadrupole Mass Spectrometry (HVE-QMS) for Ageing Management of Zr-Nb Coolant Channels**
  Radiochemistry and Isotope Group
- **Photochemotherapy by Coralyne and UVA (CUVA): A Novel Strategy for Cancer Management**
  Chemistry Group

- **Preparation and Characterization of $(U_{0.47},Pu_{0.53})O_2$ Microspheres for Test Pin Irradiation in FBTR**
  Radiochemistry and Isotope Group

May-June 2012

Articles

- **Characterization of Deformation Microstructure using Transmission Electron Microscopy: Observation of Cube Slip in γ-TiAl Alloys at Elevated Temperatures**
  Jung B. Singh
  Mechanical Metallurgy Division
- **Development of Fluidized Bed Thermal Denitration**
  Neetu A. Baveja, C.P. Shringi, Gaurav Varshney, Deepa Thomas, Sandip Bhowmick, N.K. Dandekar, M.Y. Walke and Hanmanth Rao
  Chemical Engineering Division
- **Early Detection of Coronary Heart Disease Using Peripheral Pulse Analyzer**
  G.D. Jindal, R.K. Jain, Vineet Sinha, Sadhana A. Mandalik, Bhagyashree S. Sarade, Pooja Tanawade and C.K. Pithawa
  Electronics Division
- **MetProSoft-10: Image Analysis Software for Metallographic Measurements**
  Lizy Pious, S. Kar and V.M. Joshi
  Electronics & Instrumentation Services Division
- **Passive Gamma Scanning : a Powerful Tool for QC of MOX Fuels**
  K.V. Vrinda Devi and J.P. Panakkal
  Advanced Fuel Fabrication Facility, Nuclear Fuels Group
- **Studies on Improvements in Thoria Dissolution Process for Reprocessing Application**
  C. Srinivas, Vrunda Yalmali, A.S. Pente, P.K. Wattal and S.D. Misra
  Nuclear Recycle Group

Brief Communications

- **Development of Metal – Ceramic Seals for Neutron Detectors**
  Materials Group
- **Development of Plate Thermometer (PT) or Heat Flux Measurement**
  Reactor Design & Development Group
- **Force Reflecting Telerobot**
  Design Manufacturing & Automation Group
- **H_2-F_2 Flame Reactor Technology for Nuclear Material Processing**
  Chemical Technology Group

July-August 2012

Articles

- **Bioremediation: Discovery of a Novel Alkaline Phosphatase through X-Ray Crystallography**
  Subhash C. Bihani, Shree Kumar Apte, Jean-Luc Ferrer and Madhusoodan V. Hosur
  Solid State Physics Division and Molecular Biology Division
- **Discovery of Higgs Boson: the God particle**
  A.K. Mohanty
  Nuclear Physics Division
- **DNA Repair and Recombination Proteins (Dmc1 and Rad51) from Rice *(Oryza sativa)***
  Rajani Kant Chittela and Jayashree K. Sainis
  Molecular Biology Division
- **Improved Location of Earthquakes in Sumatra Region using Gauribidanur Seismic Array Data**
  Manoj Kumar and Falguni Roy
  Seismology Division
- **Marx Generator and Reflex Triode based High Power Pulsed Microwave Source**
  Archana Sharma, Amitava Roy, Sabyasachi Mitra, Vishnu Sharma, S. Singh, Senthil Kumar, Ankur Patel, Rakhee Menon, Ritu Agrawal, A.K. Ray and D.P. Chakravarthy
  Accelerator and Pulse Power Division
- **Performance Study of Indigenously Developed CsI-Photodiode Linear Array Detectors for X-Ray Baggage Scanning Application**
  Anita Topkar, Arvind Singh, P.K. Mukhopadhyay and C.K. Pithawa and Umesh Kumar and Y. Lakshminarayana
  Electronics Division & Isotope Application Division
- **Recovery of Cesium from High Level Liquid Nuclear Waste by an Advanced Polymer Composite**
  Lalit Varshney, V.Venugopal, Amar Kumar, Tessy V. and S.D. Misra
  Radiochemistry and Isotope Group and Nuclear Recycle Group

Brief Communications

- **Design and Development of Metallic Face Seal for AHWR fueling Machine**
  Reactor Design & Development Group
- **Development of Continuous Rotary Dissolver (CRD)**
  Nuclear Recycle Group
- **Evaluation of Tripodal / Calixarene Based Diglycolamides for Actinide Extraction**
  Radiochemistry and Isotope Group
- **Integrated Δ-E Silicon Detector Telescope**
  Electronics & Instrumentation Group

- ***Meso*-and B-Substituted Pyrromethene Fluorophores as New Photo-stable Laser Dyes**
  Chemistry Group
- **Ultra High Precision Wave Length Scanning Mechanism**
  Design, Manufacturing and Automation Group

September-October 2012

Articles

- **Advanced Research on Master Curve for Safety Assessment of Reactor Pressure Vessel**
  J. Chattopadhyay, B.K. Dutta and K.K.Vaze & S.Acharyya
  Reactor Design & Development Group
- **Decontamination of Alpha Contaminated Metallic Waste by Cerium IV Redox Process**
  J. G. Shah, P. S. Dhami, P. M. Gandhi and P. K. Wattal
  Nuclear Recycle Group
- **Design, Development and Deployment of Special Sealing Plug for 540 MWe PHWRs**
  G. Sharma, S. Roy, R.J. Patel
  Refuelling Technology Division
- **Genetic Analysis of Type 2 Diabetes.**
  Suresh KG Shettigar, C. Shailaja and Ratnakar K. Kulkarni
  Pathology Unit, Medical Division
- **Non-Invasive Blood Pressure Monitor: Beat to Beat**
  Vineet Sinha, R.K. Jain, G.D. Jindal and C.K. Pithawa
  Electronics Division
- **Self Assembled Systems: Design and Drug Delivery Perspectives.**
  Gunjan Verma, Jayita Bhattacharjee and P. A. Hassan
  Chemistry Division

Brief Communications

- **Development of a 400 keV Radio Frequency Quadrupole**
  Physics Group
- **Tetrofosmin Kits for Myocardial Perfusion Imaging**
  Radiochemistry and Isotope Group
- **Ultrafast Dynamics Investigations: Development of Femtosecond Time-Resolved Infrared Spectrometer**
  Chemistry Group
- **Unveiling the Mechanism of Extreme Radiation Resistance in *Deinococcus radiodurans* by Comparative Proteomics**
  Bio-Medical Group.

BARC Scientists Honoured

Name of Scientist	:	**Dr. Srikumar Banerjee** **Homi Bhabha Chair Professor, BARC** **Former Chairman, Atomic Energy Commission**
Award	:	2012 IIM Platinum Medal in recognition of his outstanding life time contribution to metallurgy profession
Presented by	:	Indian Institute of Metals, during the 66th Annual Technical Meeting of IIM

Name of Scientists	:	**Celin Acharya and Shree Kumar Apte** **Molecular Biology Division**
Title of the paper	:	Marine cyanobacteria as suitable candidates for uranium recovery from aquatic environment
Award	:	Best Oral Presentation Award presented to Dr. Celin Acharya
Presented at	:	Indo-US workshop on cyanobacteria: Molecular networks to Biofuels, held at Lonavala, India, during December, 16-20, 2012.

Name of Scientists	:	**Anurag Kirti, Hema Rajaram and Shree Kumar Apte** **Molecular Biology Division**
Title of the paper	:	Charcterisation of three single stranded DNA binding (SSB)-like Proteins from the nitrogen-fixing cyanobacterium *Anabaena* PCC7120
Award	:	Best Poster Award presented to Anurag Kirti
Presented at	:	Indo-US workshop on cyanobacteria: Molecular networks to Biofuels, held at Lonavala, India, during December 16-20, 2012.

Name of Scientist	:	**Arbind Kumar** **Quality Assurance Division**
Award	:	National NDT Award in Recognition of his contribution in Research & Development in the field of NDE
Presented by	:	Indian Society for Non-Destructive Testing (ISNT), New Delhi, 10th December 2012.

Name of Scientist	:	**Neena Vilas Jadhav** **Radiation Biology and Health Sciences Division**
Award	:	Best Idea Award for presentation on 'Magnetic nanoparticles for combinatorial hyperthermia and radiation therapy of cancer.'
Presented at	:	International Conference on Radiation Biology (ICRB-2012) and 11th Biennial Meeting of the Indian Society for Radiation Biology held at Advanced Centre for Treatment, Research and Education in Cancer, Kharghar, Navi Mumbai, November 22-24, 2012.

V. R. Chavan
Metal Sculpture

Edited & Published by:
Scientific Information Resource Division
Bhabha Atomic Research Centre, Trombay, Mumbai 400 085, India
Computer Graphics & Layout: B. S. Chavan, SIRD, BARC
BARC Newsletter is also available at URL:http:www.barc.gov.in